TRIBHUVAN UNIVERSITY

INSTITUTE OF ENGINEERING

PULCHOWK CAMPUS

THESIS NO: PUL080MSMSE006

METAL-ORGANIC FRAMEWORKS-BASED AZOLLA BIOMASS-DERIVED CARBON COMPOSITE: PREPARATION, CHARACTERIZATION AND EVALUATION FOR REMOVAL OF METHYLENE BLUE

by

BIPANA OJHA KHATRI

A THESIS

SUBMITTED TO THE DEPARTMENT OF APPLIED SCIENCES AND CHEMICAL ENGINEERING

IN PARTIAL FULFILLMENT OF THE REQUIREMENTS FOR THE DEGREE OF MASTER OF SCIENCE IN MATERIAL SCIENCE AND ENGINEERING

DEPARTMENT OF APPLIED SCIENCES AND CHEMICAL ENGINEERING

LALITPUR, NEPAL

MAY 2026

COPYRIGHT

BOARD OF EXAMINATION AND CERTIFICATE OF APPROVAL

This thesis entitled "**Metal-organic Frameworks-based Azolla Biomass-derived Carbon Composite: Preparation, Characterization and Evaluation for Removal of Methylene Blue**" by Bipana Ojha Khatri (Roll No. PUL080MSMSE006 and T.U. Registration 5-2-20-532-2018) under the supervision of Asst. Prof. Dr. Tanka Mukhiya, Department of Applied Sciences and Chemical Engineering, Institute of Engineering, Pulchowk Campus, Tribhuvan University, is hereby submitted for the partial fulfilment of the Master of Science (M.Sc.) degree in Materials Science and Engineering. This report has been accepted and forwarded to the Controller of Examination, Institute of Engineering, Tribhuvan University, Nepal for the legal procedure.

Asst. Prof. Dr. Tanka Mukhiya
Supervisor
Department of Applied Sciences and Chemical Engineering,
Pulchowk Campus, Institute of Engineering,
Tribhuvan University, Nepal

Asst. Prof. Dr. Deval Prasad Bhattarai
External Examiner
Department of Chemistry
Amrit Campus
Tribhuvan University, Nepal

Prof. Dr. Sahira Joshi
Head of Department
Department of Applied Sciences and Chemical Engineering, Pulchowk Campus, Institute of Engineering,
Tribhuvan University, Nepal

RECOMMENDATION

This is to recommend that Ms. Bipana Ojha Khatri (Roll No 080MSMSE006, T.U. Registration No. 5-2-20-532-2018), has carried out the thesis work entitled "**Metal-organic Frameworks-based Azolla Biomass-derived Carbon Composite: Preparation, Characterization and Evaluation for Removal of Methylene Blue**" as part of the requirements for the Master of Science (M.Sc.) degree in Materials Science and Engineering under my supervision in the Department of Applied Sciences and Chemical Engineering, Pulchowk Campus, Institute of Engineering, Tribhuvan University, Kathmandu, Nepal.

She has fulfilled all the requirements laid down by the Institute of Engineering, Tribhuvan University, Nepal for the submission of the thesis work for the partial fulfillment of Master of Science (M.Sc.) degree in Materials Science and Engineering.

_____

Supervisor

Asst. Prof. Dr. Tanka Mukhiya

Department of Applied Sciences and Chemical Engineering

Pulchowk Campus, Institute of Engineering

Tribhuvan University

DECLARATION

This thesis entitled "**Metal-organic Frameworks-based Azolla Biomass-derived Carbon Composite: Preparation, Characterization and Evaluation for Removal of Methylene Blue**" is submitted to the Department of Applied Sciences and Chemical Engineering, Pulchowk Campus, Institute of Engineering, Tribhuvan University, Nepal for the partial fulfillment of the requirements for the Master of Science (M.Sc.) degree in Materials Science and Engineering. This thesis work is carried out by me under the supervision of Assistant Professor Dr. Tanka Mukhiya, Department of Applied Sciences and Chemical Engineering, Institute of Engineering, Pulchowk Campus, Tribhuvan University, Nepal.

This work was done by me originally and has not been submitted earlier, for the award of any other degree.

Bipana Ojha Khatri

Roll No. PUL080MSMSE006

T.U. Registration No. 5-2-20-532-2018

Acknowledgements

I would like to convey my heartfelt gratitude to my supervisor, Asst. Prof. Dr. Tanka Mukhiya, for his continuous advice, valuable suggestions, and constant support during this research project. His advice, suggestions and support were important in shaping our research. I am also grateful to Prof. Dr. Sahira Joshi, Head of Department, and Assoc. Prof. Dr. Ganesh Kumar Shrestha, Program Coordinator, Department of Applied Sciences and Chemical Sciences, for their support and for creating a favorable academic atmosphere in which to conduct this research.

I would like to thank Nanomaterials Laboratory for providing the required facilities to conduct the experiment. I am particularly grateful to Amrit Campus for supporting the FTIR characterization and Mr. Milan Babu Poudel from Jeonbuk National University in South Korea for providing access to FESEM characterization. I am also grateful to Asst. Prof. Purnima Mulmi for her insightful discussions and critical feedback. I am thankful to the University Grant Commission (Project number. CRIG79/80-S7T-6 UGC) for funding this work.

I would like to express sincere appreciation to Aek Narayan Kamal and Rajesh Shrestha for their invaluable support with the carbonization of the samples, which was critical to the success of this project. I would also like to thank my friends Ashman Karki, Bibek Ghimire, and Charu Gajurel for their ongoing encouragement, motivation, and help throughout this journey. Their assistance made this task more manageable and pleasurable. Finally, I would want to thank everyone who assisted in making this project a success, whether directly or indirectly.

Bipana Ojha Khatri

List of Tables

Table 1: Comparative summary of selected studies on methylene blue (MB) removal using various treatment methods 16
Table 2: Parameters of Langmuir isotherm model..... 43
Table 3: Parameters of Freundlich isotherm model 45
Table 4: R^2 values of as-prepared samples obtained from PFO kinetic model..... 48
Table 5: Parameters obtained from PSO photocatalytic kinetic model 50

List of Figures

Figure 1: Molecular structure of methylene blue 4
Figure 2: Mechanism of photocatalytic dye degradation 8
Figure 3: Photographic images of Azolla pinnata; (a) Azolla plant, (b) Azolla biomass and (c) Azolla biomass in unfavorable condition 11
Figure 4: Research design 20
Figure 5: Schematic diagram of sample preparation 22
Figure 6: Schematic diagram of UV-irradiation to methylene blue solution 24
Figure 7: XRD spectra of as-prepared carbon samples 27
Figure 8: FTIR spectra of Azolla and Azolla-derived carbon 29
Figure 9: FESEM image of a) Pristine Azolla, b) Bimetallic MOF incorporated Azolla 30
Figure 10: FESEM images of Zn-Co-Oxide/CNH@700 31
Figure 11: FESEM images of Zn-Co-Oxide/CNH@800 31
Figure 12: FESEM images of Zn-Co-Oxide/CNH@900 32
Figure 13: Elemental mapping of Zn-Co-Oxide/CNH@900 33
Figure 14: UV spectra of methylene blue after degradation using as-prepared sample 35
Figure 15: Schematic diagram of MB degradation under UV irradiation while magnetic stirring 36
Figure 16: Effect of catalyst dose on the photocatalytic degradation of 10 ppm MB 38
Figure 17: Colour changes of methylene blue over time 39
Figure 18: MB degradation (%) over different samples at 10 ppm, including dark adsorption and UV irradiation up to 120 min 40
Figure 19: Langmuir isotherm fit of four different carbon samples varying concentration of MB 42
Figure 20: Freundlich isotherm fit of four different carbon samples varying concentration of MB 44
Figure 21: Pseudo-First-Order photocatalytic kinetics varying time 47
Figure 22: Bar chart showing PFO ate constant values of as-prepared samples 48
Figure 23: Pseudo-second-order photocatalytic kinetic model varying time 51

List of Appendices

Appendix I: Herbarium of plant and its identification……65

Appendix II: Paper presentation of the work at IOE graduation conference……..67

Appendix III: Poster presentation at Third International Conference on Heritage, Innovation and Transformation……....68

Appendix IV: Photographs taken during presentation…….69

List of Abbreviations

AOP	Advanced Oxidation Process
CNH	Carbon Nano Hybrid
EDX	Energy Dispersive X-Ray Spectroscopy
FESEM	Field Emission Scanning Electron Microscopy
FTIR	Fourier Transform Infrared Spectroscopy
JCPDS	Joint Committee on Powder Diffraction
MB	Methylene Blue
MOF	Metal-Organic Framework
PAC	Pristine Azolla-derived Carbon
PFO	Pseudo-First-Order
PSO	Pseudo-Second-Order
ROS	Reactive Oxygen Species
UV-Vis	Ultraviolet-Visible Spectroscopy
XRD	X-Ray Diffraction

List of Symbols and Formula

%	Percentage
$\bullet O_2^-$	Superoxide radical anion
•OH	Hydroxyl radical
Co	Cobalt
e^-	electron
g	Gram
h	Hour
h^+	Photogenerated hole
H_2O_2	Hydrogen peroxide
L	Liter
min	Minute
mL	Milliliter
^oC	Degree Celsius
Zn	Zinc
ZnO	Zinc Oxide
θ	Angle in degree
λ	Wavelength

Abstract

This study investigates the preparation of azolla-based bimetallic metal-organic frameworks carbon composites and evaluate removal efficiency of methylene blue dye from aqueous solution. XRD analysis showed that the samples formed a well-crystalline spinel Zn-Co oxide phase in the carbon matrix. FESEM showed that the higher-temperature samples were highly porous and interconnected. The incorporation of bimetallic components into the carbon matrix was confirmed by EDX. The photocatalytic degradation of methylene blue was obtained over 90% within 60 minutes of UV irradiation. To study the adsorption isotherm of the material, Langmuir and Freundlich isotherm were plotted for the experimented data. Maximum adsorption capacity was 99.70 mg/g. The pseudo-second-order model was fitted showing the highest rate constant of 0.01376 min^{-1}. The photocatalytic degradation efficiency followed the order Zn-Co-Oxide/CNH@900 > Zn-Co-Oxide/CNH@800 > Zn-Co-Oxide/CNH@700 > PAC@900. This work suggests that azolla derived bimetallic MOF composites can be used as a promising, sustainable and cost-effective material in dye removal by photocatalytic reactions and wastewater treatment applications.

Keywords**:** Zn-Co composite, Azolla, Photocatalytic, Metal-organic frameworks, Porous Carbon, Methylene blue

Contents

COPYRIGHT ii

BOARD OF EXAMINATION AND CERTIFICATE OF APPROVAL iii

RECOMMENDATION iv

DECLARATION v

Acknowledgements vi

List of Tables vii

List of Figures viii

List of Appendices ix

List of Abbreviations x

List of Symbols and Formula xi

Abstract xii

CHAPTER 1 1

1. Introduction 1

1.1 Background 1

1.2 Dyes as major water pollutant 2

1.3 Methods of removal of dyes 4

1.4 Mechanism of photocatalytic dyes degradation 7

1.5 Nanomaterials and removals of dyes 8

1.6 Biowaste-derived carbon for dye removal 9

1.7 Azolla as sustainable carbon precursor 10

1.8 Metal-organic frameworks 11

1.9 Problem statement and research gap 11

1.10 Objectives 12

CHAPTER 2 13

2. Literature Review 13
CHAPTER 3 19
3. Materials and Methods 19
3.1 Materials 19
3.2 Methods 20
3.2.1 Research design 20
3.2.2 Plant selection 21
3.2.3 Sample collection 21
3.2.4 Preparation of metal-organic frameworks integrated azolla biomass derived carbon 21
3.2.5 Materials characterizations 22
3.2.6 Preparation of methylene blue solution 23
3.2.7 Photocatalytic methylene blue degradation 23
CHAPTER 4 26
4. Results and Discussion 26
4.1 X-ray Diffraction analysis 26
4.2 FTIR analysis 28
4.3 FESEM analysis 30
4.4 EDX analysis 32
4.5 Photocatalytic degradation of methylene blue 34
4.6 Adsorption isotherm studies 40
4.7 Photocatalytic degradation kinetics 45
CHAPTER 5 52
5. Conclusions 52
References 54

Appendix 65

CHAPTER 1

1. Introduction

1.1 Background

Water is one of the most essential natural resources for the existence of life and maintenance of ecological balance. Demand of water has been increased due to rapid population growth, urbanization and industrial development that resulted to excessive use and contamination of available freshwater resources (Water, 2020; Zou et al., 2025). Inappropriate garbage disposal, agricultural runoff, and industrial waste discharge have been the primary causes of water contamination (Sharma et al., 2024; Turner et al., 2021). When solid wastes are dumped directly of near water bodies, harmful liquids are released called leachates. There are still 2 billion people in the world who drink water contaminated with feces and other microorganisms (WHO, 2019). This poor water scenario has devastating effects particularly for young children. In fact, each year about 1.4 million children under the age of five suffer from waterborne diseases (Prüss-Ustün et al., 2019). Children develop neurological damage, cognitive dysfunction and developmental delays at even 5-10 μgL^{-1} of heavy metal such as lead (Lanphear et al., 2019). It is reported that communities living nearby poorly managed dumping sites consume fish with mercury content up to ten times the permissible limit (Chisanga et al., 2025).

When rainwater flows or irrigation water flows over the agricultural land, it carries away fertilizer, pesticides and herbicides into the water bodies such as rivers, lakes and groundwater. Due to this agricultural runoff occurs and excessive growth of algae occurs, known as eutrophication. It reduces oxygen levels and kills aquatic organisms. About 70% of freshwater is utilized in agriculture worldwide. Consequently, it leads to water quality degradation in rivers and lakes (FAO, 2020). Groundwater sources are contaminated with nitrate by about 50% due to the fertilizers used in agriculture. This causes methemoglobinemia in infants. There is 15-20% high risk of colorectal cancer in adults (Sutton et al., 2011; Ward et al., 2018). Aquatic insects are declined by up to 42% in pesticide contaminated water which severely disrupt food webs and ecosystem balance (Beketov et al., 2013). Industrial discharge further adds threat to water quality. Untreated wastewater is released directly into water resources from many factories and industries that contains synthetic dyes, organic solvents and other

harmful chemicals (Forgacs et al., 2004; Yunusa et al., 2021). From textile industry alone, over 200,000 tons of synthetic dyes are discharged into water bodies every year worldwide (Kant, 2012). These dyes are persistent to natural degradation and persist in the environment for longer period of time. Studies have shown that industrial effluents such as methylene blue dye can decrease the light penetration in water by up to 75%. Due to it, it inhibits photosynthesis by aquatic plants ultimately destroying the aquatic plant life (Yusuf, 2019). Diseases like liver damage, kidney disease and hormonal disruption are linked by 30-40% in communities living near the industrial discharge areas because of long-term exposure to industrial pollutants (Järup, 2003). The WHO has reported around 1.4 million deaths per year due to unsafe water, inadequate hygiene and poor sanitation, with industrial pollution being a major factor for contribution in developing countries (WHO, 2019).

Over 80% of the world's wastewater is released into environment without enough treatment and more than 3 billion population currently lack access to safe drinking water (Organization, 2021). Every year, water pollution is responsible for more deaths than war, terrorism and all forms of violence (Landrigan et al., 2018). This growing trend of water contamination, its harmful consequences on human health and the natural environment make it totally clear that there is urgency of effective mitigation strategies without anu further delay. All these statistics demand development of efficient water treatment and purification technology for sustainable water purification process.

1.2 Dyes as major water pollutant

The increasing growth of industries such as textiles, leather tanning, food processing, paper manufacturing and cosmetics has led to the release of high quantities of synthetic dyes into water resources (Shabir et al., 2022). Dyes are complex organic compounds which are chemically stable and resistant to degradation. So, it is particularly challenging for removal from wastewater. Synthetic dyes are one of the most hazardous pollutants among the various types of industrial pollutants due to their persistence, visibility even at very low concentrations and toxicity to living organisms. Over 800,000 tonnes of synthetic dyes are produced annually, with an estimated 100,000 different varieties currently being used commercially globally (Kusumlata et al., 2024). Among different industries, the textile industry is the largest one to

consume synthetic dyes. It is also responsible for creating the greatest volume of dye contamination in water. Approximately 10-15% of the total dyes are lost while dyeing operations and ultimately discharged into wastewater streams without enough treatment (Periyasamy, 2024).

The dyes are clearly visible even at very low concentrations as low as 1 mg. L^{-1} so, it causes significant damage in aesthetics and ecology (H. Ali, 2010). Dye molecules adsorb and also reflect sunlight entering the water which reduce light penetration and inhibits the photosynthesis of phytoplankton and aquatic plants. Fish and other aquatic species perish under hypoxic conditions caused by this disturbance of primary productivity that lowers dissolved oxygen level. Dye-contaminated water can reduce dissolved oxygen concentrations to lower than 2 mg. L^{-1} which is insufficient to support most forms of aquatic life (Ogugbue & Sawidis, 2011). Beyond ecological damage, synthetic dyes can cause serious human health risks. Many dyes and their degraded products are toxic, mutagenic and carcinogenic. Azo dyes are major used synthetic dyes that can undergo reductive cleavage in anaerobic condition to produce aromatic amines. Some of them are known to cause cancer in humans (Chung, 2016). Long term exposure to contaminated water with dyes can cause allergic reactions, skin irritation, respiratory disorders, dysfunction of the kidneys and liver, and an increased risk of bladder cancer (Lellis et al., 2019).

Methylene blue (MB) is as cationic thiazine dye with molecular formula $C_{16}H_{18}ClN_3S$ and a molecular weight of 319.85 g/mol (Information, 2021). It consists of a phenothiazine core with two dimethyl amino groups and a chloride counter ion as shown in **figure 1**. It is one of the most commonly discharged in industrial wastewater. It is widely used in paper printing, textile dyeing, and biological staining. Though it is sometimes considered less toxic in comparison to other synthetic dyes, methylene blue (MB) can cause different harmful effects in humans that include eye irritation,, nausea, vomiting, diarrhea, and methemoglobinemia at high concentrations (Yagub et al., 2014). It is highly stable in aquatic environment and is difficult to degrade by conventional treatments because of which makes it a persistent pollutant of significant concern. It imparts intense blue colour, even at trace concentrations (Jack Clifton & Leikin, 2003).

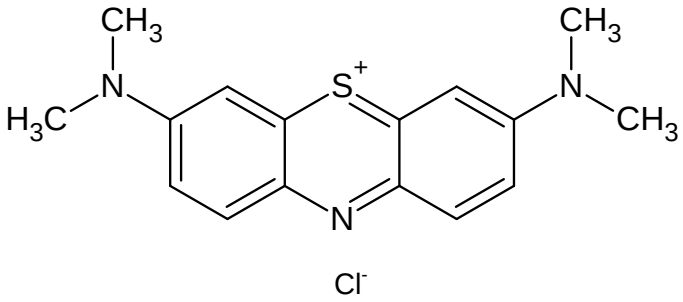

Figure 1: Molecular structure of methylene blue

1.3 Methods of removal of dyes

Over the years, various methods of treatment have been developed and are in applications. They are classified as physical, chemical and biological methods. Each of these approaches has shown different degrees of efficiency depending on the type of dye, its concentration and the properties of the wastewater. However, all of them have their own limitations which restrict their widespread and long-term applications.

I. Physical methods

a. Adsorption

Adsorption is physical methods for dye removal from wastewater. In this process, dye molecules are attracted to and held on the surface of an adsorbent. Activated carbon is commonly applied as adsorbent due to its high specific surface area and high adsorption capacity. It has been reported that activated carbon can perform up to 99% dye removal efficiencies under optimized conditions (Crini, 2006). However, commercial activated carbon is expensive to produce and hard to regenerate after use so economical large-scale application is challenging, particularly for developing countries (Singh & Fulekar, 2010).

b. Membrane filtration

Membrane filtration techniques such as nanofiltration, ultrafiltration, and reverse osmosis have been used effectively for the separation of dye molecules from the wastewater. Removal efficiency more than 95% is shown by these methods and are capable of treating large volume

of effluents (Kasperchik et al., 2012). However, this system require high initial investment costing, consume high amounts of energy and are prone to membrane fouling (Judd, 2017).

c. Coagulation and flocculation

Coagulation and flocculation include the addition of chemical agents like alum, ferric chloride, or lime to wastewater which cause dye particles to aggregate into larger clumps and can be separated by sedimentation or filtration. This method is simple to operate and comparatively cheaper. It has been investigated that it has shown 70-90% of removal efficiencies for certain types of dyes (Mcyotto et al., 2021; Saritha et al., 2017). Nevertheless, this method generates large volume of chemical sludge which require further treatment and disposal. They are generally less effective for reactive and soluble dyes (Iwuozor, 2019).

d. Ion exchange

In this method, the dye ions are replaced with less harmful ions from a resin material in wastewater. This method is highly selective and can acquire good removal efficiencies for ionic dyes. However, ion exchange resins are expensive. They have limited capacity and can be easily fouled due to the suspended particles and organic matter present in industrial wastewater (Joseph et al., 2020; Kansara et al., 2016).

II. Chemical methods

a. Chemical oxidation

In chemical oxidation, strong oxidizing chemicals are used to break down dye molecules into simpler form and less toxic compounds. Ozonation decolorize dye solutions within short contact times. However, these methods are expensive as the cost of oxidizing agents are high and require precise control of operating conditions. This may also produce toxic byproducts which require further treatments (Türgay et al., 2011).

b. Advanced oxidation processes

Advanced oxidation processes (AOPs) such as Fenton oxidation, photocatalysis and UV/hydrogen peroxide treatment usually generate highly reactive hydroxyl radicals that can

degrade a wide range of dye molecules into carbon dioxide and water. It has been reported to remove over 90% dye. Despite their effectiveness, AOPs costs high operational cost, require sophisticated equipment, sensitive to pH and other water quality parameters. It also may generate harmful intermediate products during degradation (Bethi et al., 2016).

c. Photocatalysis

Photocatalysis is a process in which a semiconductor material like titanium dioxide and zinc oxide is activated by ultraviolet or visible light to generate reactive species to degrade dye molecule. This methods has attracted researchers due to its potential for complete mineralization of dyes without producing secondary pollutants (Chong et al., 2010). But it is limited by the need of artificial light sources. It is difficult to recover the catalyst after treatment and efficiency reduces in turbid or highly concentrated wastewater (Nazri & Sapawe, 2020).

III. Biological methods

a. Biodegradation

Dyes molecules are converted into simpler form from complex with the help of microorganisms like bacteria, fungi and algae. These final products are less harmful. Certain species of fungi like white rot degrade synthetic dyes into simpler form through their extracellular enzymes such as laccase and peroxidase (Forgacs et al., 2004). Biodegradation is an environmentally friendly and cost-effective method. Despite of this advantage, it has limitations. It is a slow process and is highly sensitive to changes in temperature, pH, and the presence of toxic compounds. It is also ineffective for such dyes that are resistant to microbial attack, such as azo dyes under aerobic conditions (I. Ali, 2010).

b. Phytoremediation

Phytoremediation uses plant-derived materials to absorb, accumulate of degrade pollutants from wastewater. Some aquatic plants such as azolla, duckweed and water hyacinth have shown an ability to uptake and reduce dye concentration in water (Amalina et al., 2022; Jeffrey et al., 2025; Sundararaman et al., 2021). This is low cost, environmentally sustainable and eco-friendly method. However, its limitations are slow treatment rates, dependency on climate and

seasonal conditions, requirement of large space and the problem of disposing dye-laden plant biomass after treatment.

c. Biosorption

Biosorption is passive uptake of dye molecules by non-living biologically derived materials like agricultural wastes, algae biomass, and plant residues. It has gained quite good attention as a promising alternative to conventional adsorption because of the wide availability and low cost of biosorbents (Torres, 2020). In spite of having different advantages, they generally have lower adsorption capacities compared to activated carbon. They have limited reusability and their performance can be significantly affected by competing ions and changing pH levels in real wastewater.

Despite the availability of a wide range of method to remove dye, no single current technique has proven to be completely adequate for practical large-scale application. Physical methods are costly and difficult to regenerate. Membrane filtration has limitation of fouling and high energy demands. Chemical methods including oxidation and AOPs involve high operational costs and toxic byproducts. Biological methods are slow, sensitive to operative conditions, and ineffective against many recalcitrant synthetic dyes. Furthermore, most of these techniques merely transfer dye pollutants from one phase to another rather than completely eliminating them, leading to secondary pollution problems (Lellis et al., 2019). The generation of high volumes of sludge, the requirement of skilled operation, and lack of cost-effectiveness at industrial scale remain long-lasting challenges (Crini & Lichtfouse, 2019). These limitations in spite of having several advantages collectively highlight the pressing need for the development of novel, low-cost, sustainable, eco-friendly materials and methods for the removal of dyes from wastewater.

1.4 Mechanism of photocatalytic dyes degradation

The mechanism of photocatalytic dye degradation starts when a semiconductor photocatalyst absorbs light of required energy equal to or greater than its bandgap energy. This causes electron in the valence bond of the catalyst excited and jump to the conduction band as shown in **figure 2**. It generates electron-hole pairs on the surface of photocatalyst (Ajmal et al., 2014).

The generated positive holes react with water molecules or hydroxide ions to generate highly reactive hydroxyl radicals on the surface of photocatalyst (•OH). Similarly, the excited electrons react with dissolved oxygen producing superoxide radical anions ($•O_2^-$). These reactive oxygen species are very strong oxidants. They can degrade and attack almost all organic dye molecules (Nosaka & Nosaka, 2017). The hydroxyl radicals break down the colour of the dye molecule, which is due to the chromophore group, by splitting the conjugated aromatic ring system and thus breaking down the molecule into smaller compounds. These intermediates are then oxidized further until they are completely mineralized. After oxidization, carbon dioxide, water, and inorganic ions are formed as the final non-toxic products (Konstantinou & Albanis, 2004).

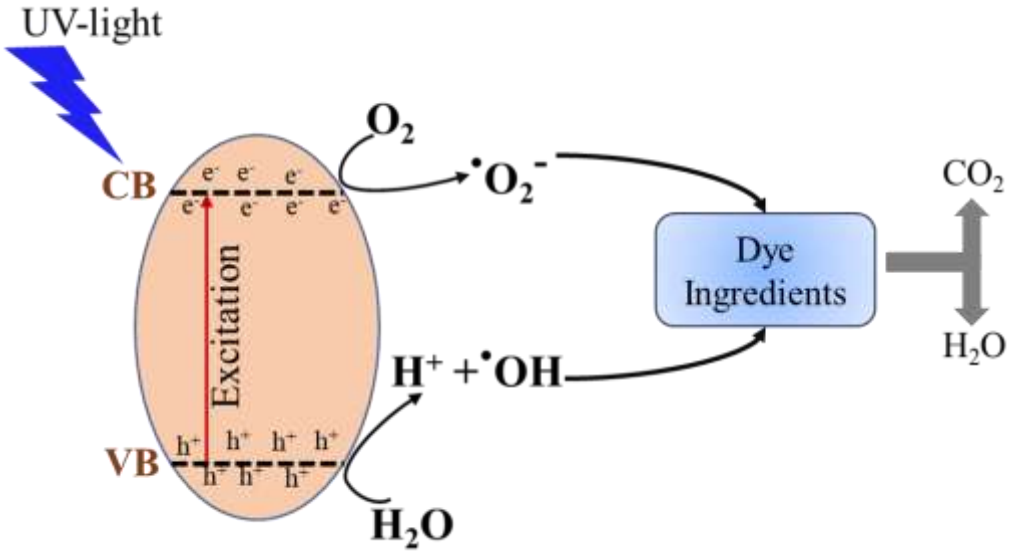

Figure 2: Mechanism of photocatalytic dye degradation

1.5 Nanomaterials and removals of dyes

Nanomaterials are materials with 1-100 nanometers (nm) in one of the dimensions which exhibit unique physical, optical, electrical and chemical characteristics compared to their bulk materials (Dagdag et al., 2024). Nanomaterials has gained a significant attraction in modern civilization in different fields including wastewater treatment (Jangid & Prabhu Inbaraj, 2021). One of the attractive features of nanomaterials in wastewater treatment is high specific surface area. Therefore, nanomaterials can remove pollutants from wastewater more efficiently than

their corresponding bulk materials. Nanomaterials can be fabricated in different nanoarchitecture and composition as per required. Moreover, specific nanomaterials can be designed and developed for selective removal of more toxic pollutant (El-Fattah et al., 2024). Nanomaterials have been applied in different forms such as particle, membrane or in other forms to remove conventional to emerging pollutants from wastewater (Boulkhessaim et al., 2022). In addition to other pollutants, nanomaterials, in general, possess high efficiency of removing dyes from wastewater due to their unique physicochemical characteristics. The adsorptive capacity of nanomaterials is very high due to their high specific surface area. Abundant functional groups can be developed in the surface of nanomaterials which binds particular dyes. Some nanomaterials such as ZnO and TiO_2 are responsible for photocatalytic degradation of dyes (Ghamarpoor et al., 2024). Carbon nanomaterials and their nanocomposites have emerged as efficient and low-cost materials for removal of dyes from wastewater (Patel et al., 2024).

1.6 Biowaste-derived carbon for dye removal

Carbon materials have become an important material in wastewater treatment because of its high surface area, chemical stability and good affinity towards organic pollutants (Tan et al., 2015). Activated carbon, biochar and carbon nanomaterials have been extensively investigated as dye adsorption materials from aqueous solutions. The surface functional groups and porous structure of these materials allow them to effectively interact with dye molecules via hydrogen bonding interaction, π-π interaction and electrostatic interaction (Ali, 2012). However, carbon nanomaterials are primarily derived from fossil resources causing rapid depletion of resource and environmental pollution. Another primary drawback is that these nanomaterials mainly act as adsorbents, transferring dyes from water to solid phase rather than degrading them, which created secondary wastes (Tan et al., 2015). Regeneration of spent carbon is often energy-intensive, costly, and loss over repeated cycles. In addition, adsorption efficiency can be affected by pH, competing ions, and high concentration of dye. Also, pore blockage and surface fouling further reduce long-term effectiveness (Crini & Lichtfouse, 2019). These challenges limit large-scale applicability and have driven the interest towards functionalized and composite carbon materials with enhanced and multifunctional dye removal capabilities.

Biomass carbon materials have recently been considered as alternatives to conventional carbon materials resources because they are cheap, eco-friendly and renewable (Ioannidou & Zabaniotou, 2007). It was found that there are a number of carbon precursors, such as plant biomass, agricultural wastes, and algae, that have been widely studied. These sources are rich in carbon and also naturally rich in heteroatoms. The heteroatoms (N, O and S) and surface functional groups increase the surface reactivity and adsorption capacity, as well as interaction with organic pollutants (Tan et al., 2015). Biomass carbon is a more sustainable and cost-effective activated carbon than commercial activated carbon in the treatment of wastewater. However, they often need additional modification and functionalization to realize their ideal performance and expand their application (Crini & Lichtfouse, 2019).

1.7 Azolla as sustainable carbon precursor

Azolla belonging to the Salviniaceae family, is heterosporous rapidly growing fern. It doubles its biomass in 2-5 days under optimal condition. Azolla can produce up to 10 kg of biomass per 100 m^2 per day (Alebachew Chekol et al., 2024; Rashad, 2021). Due to this capacity, it has been a subject of interest as one of the most promising sustainable bioresources. It is also called green gold mine because of this quality (Korsa et al., 2024; Vijayan et al., 2024). In addition, Azolla possess multiple applications such as biofertilizer, carbon dioxide sequestration, methane production reduction. Azolla forms a mutually beneficial relationship with *Anabaena azollae* in order to promote effective nitrogen fixation (Pereira, 2017; Peters & Mayne, 1974). that produce dense mats on the surface of freshwater. It grows rapidly on the surface of fresh water in minimal nutrients and can be easily harvested. Due to its exceptionally high growth rate and ability to fix atmospheric nitrogen through symbiotic cyanobacteria, it is rich in carbon and heteroatoms, especially nitrogen and oxygen. The unique chemical composition of *Azolla* makes it a suitable precursor for the synthesis of functional carbon materials (Bhuvaneshwari & Singh, 2015)

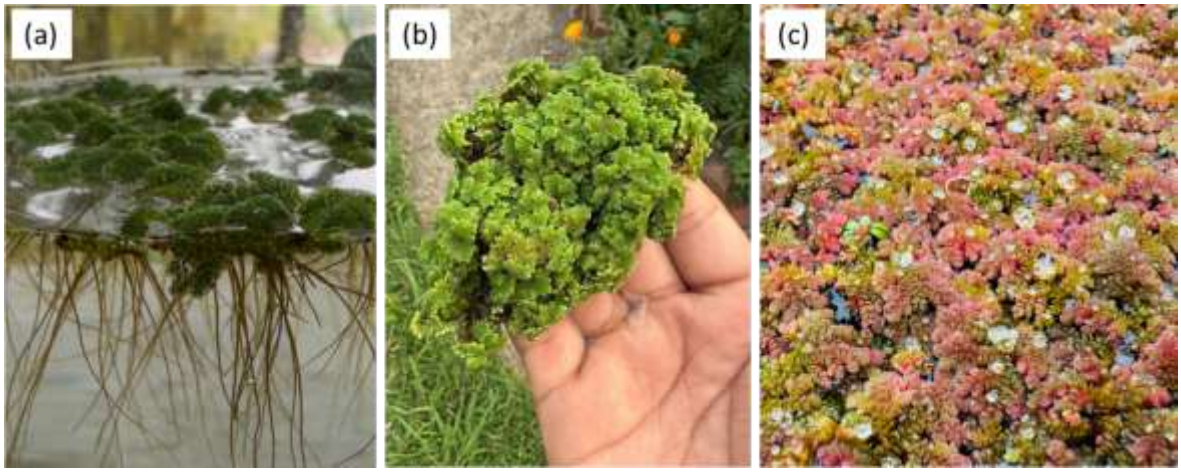

Figure 3: Photographic images of *Azolla pinnata*; (a) Azolla plant, (b) Azolla biomass and (c) Azolla biomass in unfavorable condition

1.8 Metal-organic frameworks

Metal-organic frameworks (MOFs) are porous crystalline materials formed by network of metal ions or clusters with organic molecules (Furukawa et al., 2013). MOFs have been used for a variety of applications including storage of energy, catalysis, sensing, and remediation of the environment due to their extremely high surface area, tunable pore structure, and a wide range of chemical functionality. MOFs are versatile materials, being able to be varied in composition and structure. However, these merits are not sufficient for the use of MOFs in aqueous wastewater treatment due to the low chemical stability, water resistance, and recovery and reusability. Most MOFs have a tendency to deteriorate or lose their structure upon extended water or reactive contact (Kreno et al., 2012). This has spurred the development of modifications to MOFs and even into more stable derivatives.

1.9 Problem statement and research gap

Extensive research has been carried out on the removal of synthetic dyes from wastewater using different adsorbents and photocatalysts including activated carbon, biochar, metal oxides, and metal-organic frameworks, individually. However, despite the growing interest in composite materials for enhancement in dye removal efficiency, the synthesis and application of MOF-based carbon composites specially derived from azolla biomass has not been reported

in literature yet. This shows a significant and unexplored research gap which is the aim of present study.

Azolla is and adequately available aquatic fern and low-cost biomass that is rich in carbon content. It has been extensively explored and studied for its bioremediation potential. However, its potential as a precursor for the carbon synthesis intended for use in composite catalyst and adsorbents for dye removal has not been explored. On the other hand, metal-organic frameworks are well known for their exceptionally high specific surface area, tunable porosity, and ability to ensure the uniform distribution of metal or metal oxide nanoparticles at the nanoscale level. These are all highly desirable properties for both adsorptive and photocatalytic applications (Zhang et al., 2019). Despite these attractive properties, the combined MOF-derived structures with azolla biomass-derived carbon into a single composite material for the dye removal application has not been investigated till today. Therefore, the present study is the first attempt to synthesize, characterize, and evaluate a MOF-based azolla biomass-derived carbon composite for the removal of methylene blue, with the aim of filling this important gap in the existing literature.

1.10 Objectives

General objective

To develop bimetallic Zn-Co-MOF-derived carbon composite from Azolla biomass for the methylene blue removal.

Specific objectives

To synthesize Azolla biomass-based carbon

To synthesize zinc-cobalt MOF assimilated azolla derived carbon composite

To characterize as-prepared material by XRD, FESEM, EDX, FTIR.

To evaluate the removal efficiency of methylene blue by using as-prepared carbon.

CHAPTER 2

2. Literature Review

Synthetic dyes are non-biodegradable, toxic and chemically stable and the treatment of dye contaminated wastewater is still a great challenge to the environment. Of these, methylene blue (MB) is widely applied in a variety of industries including textile, cosmetics, and paper, and can be released into water body at non-detrimental concentrations, yet it can still have an impact on the photosynthetic activity and water quality. The mutagenic and carcinogenic properties of MB and its degradation have been reported (Forgacs et al., 2004; Yagub et al., 2014). These concerns highlight the importance of the need for effective, sustainable and economically viable treatment methods.

The traditional techniques of dye removal such as physical, chemical and biological have been used, with each having its drawbacks. Due to the high surface area and adsorption efficiency, the adsorption process using activated carbon has been extensively studied. But it is limited in practicality due to high cost, energy intensive regeneration and secondary waste generation (Ali, 2012). Although dyes can be partially removed by chemical treatments (coagulation, flocculation and oxidation), these processes may generate unwanted side products and consume significant amounts of chemicals, and biological treatments are ineffective for MB because of the dye's chemical stability and resistance to microbial degradation (Crini & Lichtfouse, 2019; Sharma & Kaur, 2018). Although membrane-based processes have been proven to be very effective separation technologies, they are costly, fouling and require a high amount of energy, and hence cannot be widely used.

There are several reasons for the development of carbon materials using biomass: they are inexpensive, sustainable, and effective adsorbers. Agricultural residues, algae and plant biomass have been converted to biochar or activated carbon with hierarchical porosity and functional surface groups that interact with dye molecules through hydrogen bonding, π-π interactions, and electrostatic forces (Meng et al., 2025; Tan et al., 2015). The presence of heteroatoms (N, O, and S) further boosts adsorption and catalytic ability (Fang et al., 2025). However, biomass-based carbon is a main adsorbent and can remove pollutants from a liquid

phase to a solid phase, but it does not degrade then. It is also affected by operational parameters like pH, ionic strength and pollutant concentration (Crini & Lichtfouse, 2019). Recent research has thus been directed towards functionalizing biomass carbons or incorporating catalytic components into them to achieve both adsorption and degradation.

Metal-organic frameworks are versatile porous materials having high surface area and tunable pore structure and chemical functionality that are applicable to adsorption and catalysis applications. MOFs can be engineered to maximum the interaction if the dye molecules with the MOF through electrostatic, π-π, and coordination interaction (Furukawa et al., 2013; Kreno et al., 2012). However, the use of these in an aqueous system is restricted due to poor water stability, and issues of recovery and reuse (Burtch et al., 2014). Mitigating these drawbacks, MOFs can be thermally transformed into MOF-derived carbon materials and enhanced porosity and metal derived active sites, but with increased stability and conductivity. Zn-based MOF-derived carbon composites have exhibited higher adsorption capacity and photocatalytic activity for MB removal, which have been attributed to the synergistic effect of the two, while the bimetallic MOF-derived carbons have multiple active centers and facilitate the transfer of electrons, leading to faster degradation of the dye (Li et al., 2024; Zhang et al., 2020).

Synergistic effects have been observed by integration of the biomass-derived carbon and MOF derived materials, which resulted in the enhancement of the photocatalytic performance. For these hybrid systems, the MOF part acts as a photocatalyst while the biomass carbon acts as a conductive pathway and extra adsorption sites. Recent reports indicated that the biomass@MOF based carbon composites possess higher efficiency of MB degradation than individual components, due to the enhanced light absorption, charge separation and the increase in the active sites (Li et al., 2025; Zhang et al., 2020). Photocatalytic degradation is mediated by ROS, including OH, which are produced by the degradation of MB molecules, and the addition of carbon matrices decreases the recombination of electron-hole pairs, which increases the photocatalytic (Li et al., 2024).

Azolla is especially fascinating as a biomass source because it has a high degree of nitrogen and carbon content, high growth rates and is rich in heteroatoms that increase catalytic activity and surface interactions. The MOF integration can be achieved with the help of the stable and

high surface area carbon derived from Azolla as a substrate (Das et al., 2018; Kuppusamy et al., 2026). But its use with bimetallic MOF-derivative carbon in MB photocatalytic degradation is still under studied and has a remarkable research gap. The production of such composites is expected to offer sustainable, efficient, and cost-effective solutions to the treatment of wastewater that is contaminated with dyes.

So far, although much work has been done on biomass carbon and MOF materials, most of the studies have been carried out separately in the area of adsorption or photocatalysis. Although a lot of research has been performed on biomass carbon and MOF materials, most of the works have been conducted separately, both in the field of adsorption and in the field of photocatalysis. It is noteworthy to note that by synthesizing the bimetallic MOF carbon composites derived from the azolla, high adsorption and high photocatalytic activity can be obtained, which is a gap in the literature. The present study aims to explore this approach to advance functional biomass-based materials for effective MB removal.

The removal of methylene blue (MB) from wastewater using different treatment processes such as adsorption, photocatalysis, membrane filtration, advanced oxidation processes (AOP), and combination of these have been explored. Selected literature on MB removal is summarized in **table 1** in which the adsorbent or material used, the operational conditions (pH, contact time), the maximum adsorption capacity, the removal efficiency and the isotherm and kinetic models used are presented. In most of the adsorption studies, the pseudo-second order kinetic model was found to be the best fit and the Langmuir or Freundlich isotherm models were found to be the best fit, indicating that the chemisorption is the major process involved in the removal process. The results presented in this study show this diversity of approaches and materials with which to investigate the removal of MB, and the necessity of using low cost, efficient and reusable adsorbents.

Table 1: Comparative summary of selected studies on methylene blue (MB) removal using various treatment methods

Adsorbent / Material	**pH**	**Contact Time**	**Max Capacity (mg/g)**	**Removal Efficiency**	**Isotherm Model**	**Kinetic Model**	**Ref.**
KOH/$FeCl_3$ modified corncob biochar / alginate beads (MCB/ALG)	ND	ND	1373.49	>85% (5 cycles)	Langmuir	Pseudo-2nd order	(H. Liu et al., 2023)
Sulfonic acid-modified magnetic sugar biochar	11	ND	869.6	ND	Langmuir	Pseudo-2nd order	(Jiang et al., 2023)
Al_2O_3 nanoparticles on silica sand (SSC-Al2O3)	6	75 min	ND	95.33%	Freundlich	ND	(Hussein & Rasheed, 2025)
Magnetic NaOH-impregnated bamboo charcoal	ND	ND	497.51	ND	ND	Pseudo-1st order (catalytic)	(Q. Liu et al., 2023)
Commercial filter paper	ND	ND	ND	ND	Freundlich	Pseudo-2nd order	(Bogyor et al., 2025)
Chestnut shell activated carbon +	ND	300 min	1635 (sat.)	92%	Freundlich	Pseudo-2nd order	(An et al., 2022)

pyrolytic snail shells (MCS3-1)							
Fennel seed (*Foeniculum vulgare*) biochar (CO_2 activation)	ND	ND	22-43	ND	Langmuir / Freundlich	Pseudo-2nd order	(Paluch et al., 2024)
Fir bark-derived activated carbon (ACFB)	7	180 min	330	ND	Freundlich / Temkin	Pseudo-2nd order	(Luo et al., 2019)
Ball-mill modified biochar (BRB)	8	90 min	50.27	99.78%	Langmuir	Pseudo-2nd order	(Wang et al., 2023)
ZnO-RGO nanocomposite (3 synthesis methods)	8	60 min	104.5	95%	Langmuir	Pseudo-2nd order	(Hussein et al., 2025)
ZnO-loaded modified sugarcane bagasse biochar (Zn-BCs)	ND	50 min	ND	99.6%	ND	ND	(Ma et al., 2025)
Cellulose nanocrystals / carboxymethyl cellulose /	Alkaline	120 min	38.3-76.5	79.9-94.5%	Freundlich	Pseudo-2nd order	(Ibrahim et al., 2024)

zeolite membrane							
EuVO4/g-C3N4 mesoporous nanosheets (EVC-2)	ND	30 min	ND	~100%	Langmuir	Pseudo-2nd order	(Ran et al., 2022)
MIL-100(Fe)/GO composite (1M8G)	ND	210 min	60.8	95%	Langmuir	Pseudo-2nd order	(Wei et al., 2024)
Activated carbon-ZnO-ammonia composite (AC-ZnO-NH3)	9	180 min	106.38	97.4%	Langmuir / Freundlich / Temkin	Pseudo-2nd order	(Alprol et al., 2025)
Zeolites (NH4BETA, NH4ZSM-5, NaY) under UV irradiation	ND	180 min		ND	Freundlich	ND	(Rakanović et al., 2022)

ND = Not determined/reported. Removal efficiency values are as reported under optimal conditions in each study.

CHAPTER 3

3. Materials and Methods

3.1 Materials

Apparatus

Beaker, volumetric flask, conical flask, measuring cylinder, funnel, centrifuge tubes, and Eppendorf tubes were used.

Chemicals

Cobalt nitrate hexahydrate [$Co(NO_3)_2 \cdot 6H_2O$, ≥ 98%, Junsei Chemical Co.,Ltd.)], zinc nitrate hexahydrate [$Zn(NO_3)_2 \cdot 6H_2O$), ≥ 98%, SRLchem), and 2-methylimidazole (99%, Sigma-Aldrich), Methanol (99%, Qualigens), Methylene Blue (Loba Chemie). The materials were used as received without further purification was used as the solvent.

Instruments

Weighing balance (Ohaus E01140 Explorer), grinder, Tube furnace (Kejiafurnace), hot air oven (Gallenkamp), Muffle furnace, UV Source (Omnicure Series 1500), centrifuge machine (Biobase), and UV-vis spectrophotometer (UV-2600i, Shimadzu) were used.

Biomass precursor

The plant taken as biomass precursor was *Azolla pinnata*. It is classified as:

Kingdom: Plantae
Subkingdom: Pteridobiotina
Phylum: Tracheophyta
Class: Polypodiopsida
Order: Salviniales
Family: Salviniaceae
Genus: *Azolla*
Species: *pinnata* R. Br.

3.2 Methods

3.2.1 Research design

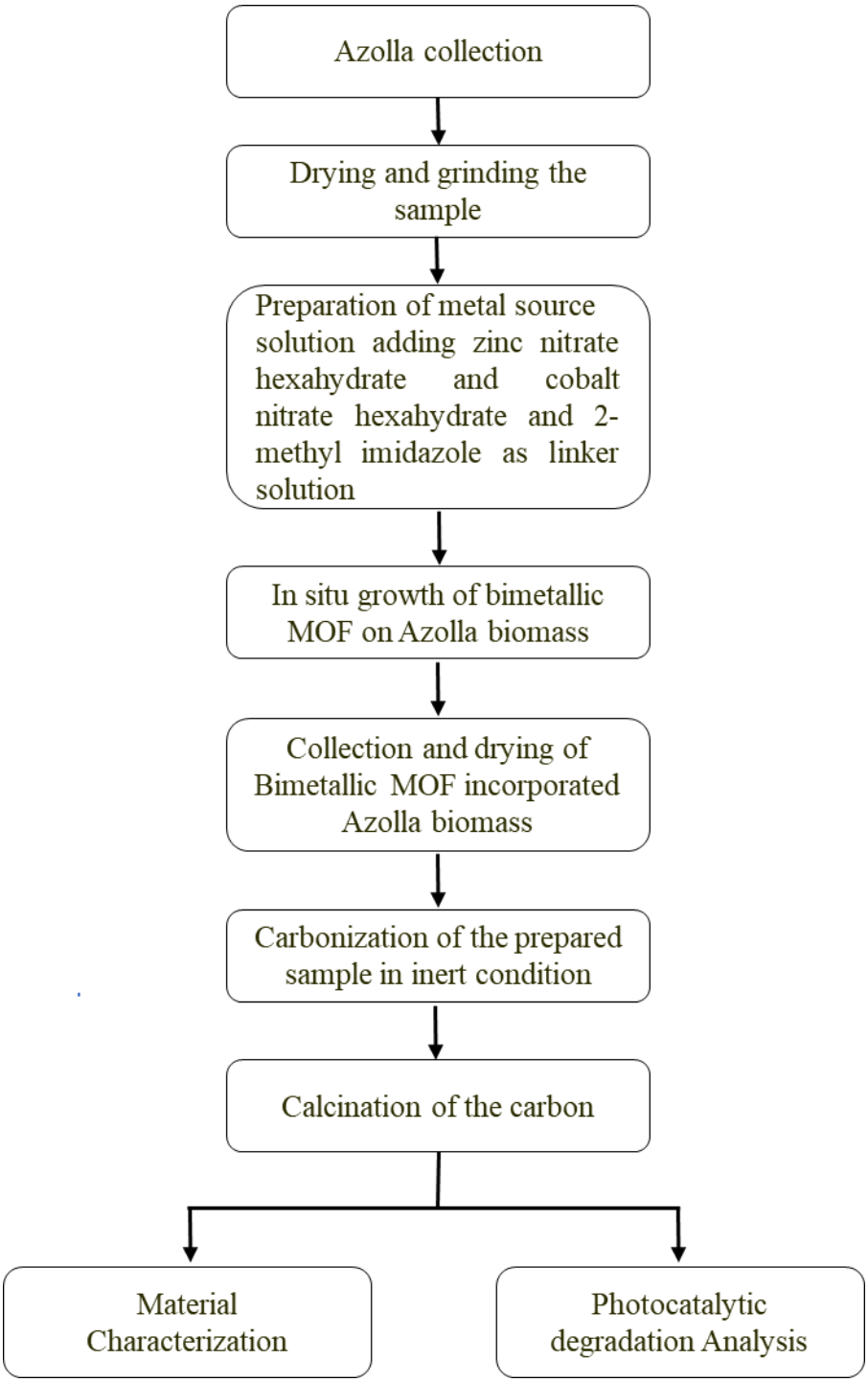

Figure 4: Research design

3.2.2 Plant selection

Azolla was selected as the biomass precursor for the preparation of carbon sample due to its exceptional property of rapid growth, easy availability, and low cost (Hamdan & Houri, 2022). According to different studies that improve adsorption of pollutants such as dyes (Lu et al., 2017). Also, its high biomass yield and eco-friendly nature make it a suitable precursor for designing and developing efficient and sustainable materials for wastewater treatment.

3.2.3 Sample collection

The sample, i.e., *Azolla pinnata,* commonly known as mosquito fern, was collected from the nearest farm located at Godawari, Lalitpur, Nepal. The herbarium of the selected plant species was prepared as shown in **appendix 1** and identified at National Herbarium and Plant Laboratories (Lath), Godawari, Lalitpur, Nepal.

3.2.4 Preparation of metal-organic frameworks integrated azolla biomass derived carbon

The schematic diagram of the sample preparation is shown in **figure 5**. Initially, fresh azolla was taken, washed, sun-dried for 3 days and also oven dried in 60 °C for 48 h. Then the dried azolla was crushed into powder by mechanical grinder. 5 g of finely powdered Azolla biomass was taken in a conical flask. 4.91 g of cobalt nitrate hexahydrate, 1.487 g of zinc nitrate hexahydrate and 250 mL of methanol were added into the conical flask. It was then subjected to magnet stirring for 3 h. 9.85 g of 2-methylimidazole was dissolved in 200 mL of methanol by magnetic stirring for 15 min and added into conical flask containing azolla and shaken for 2 min. It was left undisturbed for 20 h at room temperature. Next day, it was centrifuged at 5000 rpm for 10 min and separated the residue. The obtained residue was oven dried at 60 °C for 24 h.

Figure 5: Schematic diagram of sample preparation

2 g of prepared sample was carbonized at 900 °C for 2 h in a tube furnace in the inert atmosphere of nitrogen gas. 0.04 g of carbon sample was subjected to calcination at 410 °C for 20 min in muffle furnace before testing photocatalytic dye degradation. For comparison, the sample was carbonized at 800 °C and 700 °C. Pristine azolla biomass was also carbonized at 900 °C in similar condition.

3.2.5 Materials characterizations

X-ray Diffraction (XRD)

Crystallinity and identification of as-prepared samples were examined by Powder XRD using X-ray diffractometer (XRD, Rigaku, Cu Kα (λ = 1.54056 A, 40 kV, and 40 mA). The

diffraction patterns were taken in a 2θ range of 10° to 80°. XRD is used to identify the crystallinity, phase composition and structural properties (Kiani, 2023).

Field Emission Scanning Electron Microscopy and EDX

The surface morphology and microstructure of the materials was analyzed by field emission scanning electron microscopy (FESEM, JEOL JSM). FESEM gives high-resolution images by using a focused beam of electrons emitted from a field emission source (Nandee et al., 2024).

Attenuated total reflectance-Fourier transform infra-red (ATR-FTIR) spectroscopy

Fourier transform infrared (FTIR) spectroscopy was performed by a PerkinElmer Spectrum IR version 10.6.2 spectrophotometer in attenuated total reflectance (ATR) mode. This approach is done to analyze the presence of functional groups in the material (Berthomieu & Hienerwadel, 2009). The spectra were taken within the wavenumber range of 4000-400 cm^{-1} after the deposition of as-prepared samples onto a diamond crystal.

3.2.6 Preparation of methylene blue solution

In a 1000 mL volumetric flask, 0.1 g of methylene blue was dissolved in 1000 mL distilled water to prepare 100 ppm methylene blue solution. It was then used as a stock solution. Different concentrations of methylene blue (2, 4, 6, 8, 10 ppm) were prepared for the calibration of methylene blue from the stock solution. Similarly, for adsorption and photocatalytic performance, 5, 10, 20, 40 ,50 and 60 ppm concentrations of methylene blue were prepared by serial dilution.

3.2.7 Photocatalytic methylene blue degradation

Initially, 50 mL 0f 10 ppm methylene blue solution was taken in 100 mL beaker and 0.01 g of prepared carbonized sample at 900 °C was added to it. It was then stirred magnetically in dark for 30 min. 4 mL of methylene blue solution was collected in 15 mL centrifuge tube from the beaker er for UV-vis analysis. Further the solution with carbon sample was exposed in UV (300-500 nm) for 15 min along with magnetic stirring as shown in **figure 6**. After 15 min, again 4 mL of methylene blue solution from the beaker was collected in centrifuge tube. This process was repeated for 30, 45, 60, 90 and 120 min of UV exposure to the methylene blue

solution containing carbon sample. UV-vis spectroscopy analysis of obtained methylene blue solution was done. For comparison, carbon sample carbonized at 700 °C and 800 °C and pristine azolla carbon carbonized at 900 °C were used for photocatalytic degradation in 10 ppm methylene blue solution.

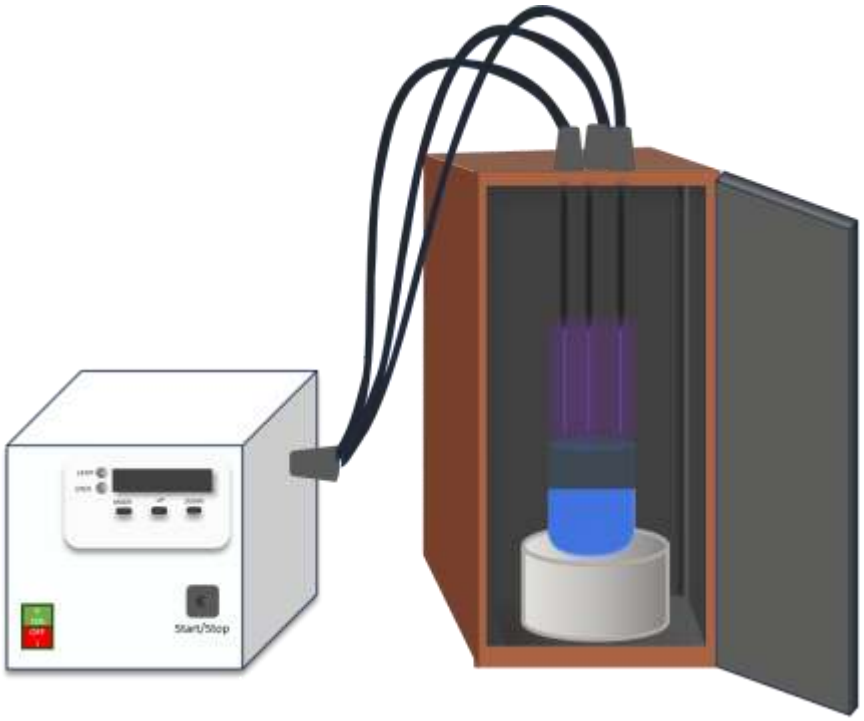

Figure 6: Schematic diagram of UV-irradiation to methylene blue solution

Similarly, all four carbon samples were employed for photocatalytic degradation in different concentrations (5 ppm, 20 ppm, 40 ppm) taking 25 mL methylene blue solution and 0.005 g carbon sample for 30 min dark adsorption and 30 min UV exposure. For the UV analysis the absorbance of methylene blue was taken in the wavelength range from 550 nm to 750 nm with maximum wavelength ~664 nm. The determination is based on the Beer-Lambert law, which states that the absorbance of a solution is directly proportional to the concentration of the absorbing species. A calibration (quantitation) curve was prepared using standard MB solutions of known concentrations from 2 ppm to 10 ppm, giving a linear relationship between absorbance and concentration;

$$A = mC + b \quad [1]$$

Where; A = absorbance of methylene blue solution

m = slope of calibration curve

C = Concentration of methylene blue

b = intercept of the calibration curve

The concentrations of the collected samples were calculated by substituting the measured absorbance values into this equation. The degradation process was expressed as the normalized concentration ratio C/C_0, where C_0 is the initial dye concentration and C is the concentration at time *t*. The degradation efficiency was evaluated using the ratio C/C_0. The percentage degradation of methylene blue was calculated by using formula:

$$\% \text{ Degradation} = \frac{C_0 - C}{C_0} \times 100\ \% \qquad [2]$$

Where, C_0= Initial dye concentration

C= Dye concentration at a given irradiation time

The same experimental procedure was repeated for all four azolla-derived carbon samples.

CHAPTER 4

4. Results and Discussion

4.1 X-ray Diffraction analysis

Figure 7 represents the X-ray Diffraction (XRD) patterns of as-prepared carbon samples. The XRD pattern of PAC@900 displayed two broad and relatively weak diffraction peaks centered at approximately $2\theta = 26°$ and $2\theta = 43°$, which correspond to the (002) and (100) crystallographic planes of graphitic carbon, respectively. The broad and low-intensity nature of these peaks is characteristic of an amorphous to partially graphitic carbon structure, indicating that the Azolla biomass-derived carbon obtained at 900°C possesses a disordered carbon framework with limited long-range crystalline order (Marsh & Reinoso, 2006). The presence of the (002) reflection confirms the existence of stacked graphene-like layers within the carbon structure, while the (100) reflection is associated with the in-plane ordering of the carbon hexagonal lattice. The broad humps rather than sharp peaks confirm the predominantly amorphous nature of PAC@900, which is typical of biomass-derived activated carbon materials (Yahya et al., 2015).

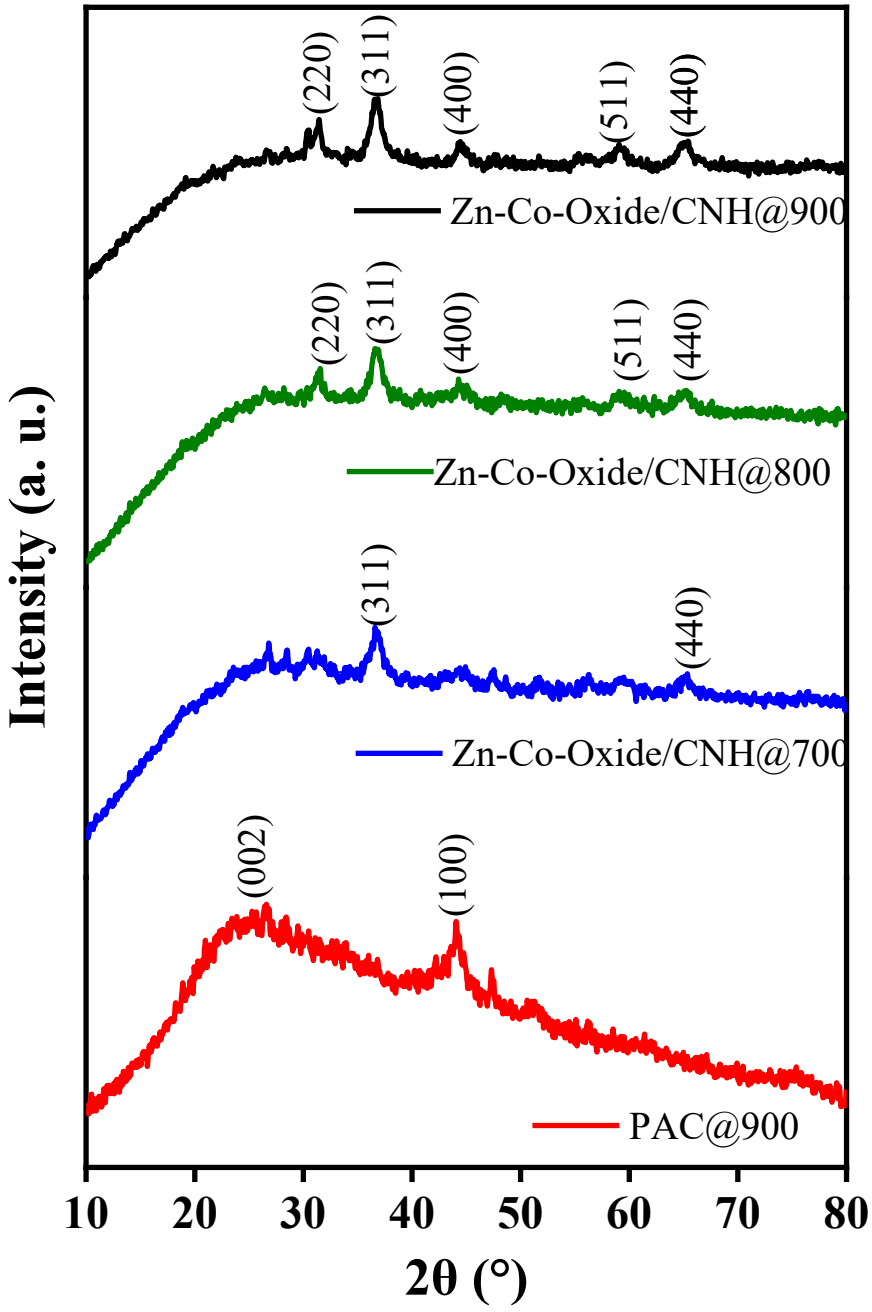

Figure 7: XRD spectra of as-prepared carbon samples

In the XRD pattern of Zn-Co-Oxide/CNH, it shows common peaks at 2θ of about 36° and 65° corresponds to the plane (311) and (440) respectively whereas few more peaks are prominent in the carbon composites at higher temperature (800 °C and 900 °C). They are at about 31°,

44° and 59° which corresponds to the plane (220), (400) and (511) respectively diffraction planes of Co_3O_4 (JCPDS No. 42-1467) (Mukhiya et al., 2020).

4.2 FTIR analysis

Figure 8 depicts the FTIR spectra of pristine Azolla powder, pristine Azolla carbon, and zinc-cobalt integrated carbons prepared at different carbonization temperatures from 700 °C to 900 °C. FTIR was done to study the presence of functional groups and detect the chemical transformations during carbonization and metal-carbon bond formations. The spectrum of pristine Azolla powder showed a broad peak at ~3316 cm^{-1} which corresponds to O-H stretching from hydroxyl groups in cellulose, hemicellulose, and adsorbed water, while peaks at ~2924 cm^{-1} corresponds to C-H stretching of aliphatic -CH_2 /-CH_3 groups. The band around 1635 cm^{-1} is probably related to C=C stretching vibrations of the aromatic structure and may be due in part to H-O-H bending of the water molecules on the surface. The polysaccharide C-O stretching was found around 1049 cm^{-1} and skeletal vibrations in the fingerprint region were found in the vicinity of 670 cm^{-1}. The presence of rich concentration of oxygenated functional groups in azolla biomass is supported from these observations, which are in line with the previous report of the oxygenated functional groups found in lignocellulosic materials (Pandey, 1999).

The FTIR spectrum of pristine Azolla carbon showed a significant reduction in O-H and C=O bands after carbonization. It indicates decomposition of unstable oxygenated groups. The presence of a band around 1635 cm^{-1} suggests the formation of aromatic C=C bond, depicting partial graphitization of the carbon matrix. This transformation aligns with previous studies showing that carbonization removes oxygenated functionalities and produces stable aromatic networks suitable as a matrix for metal incorporation (Sevilla & Fuertes, 2009).

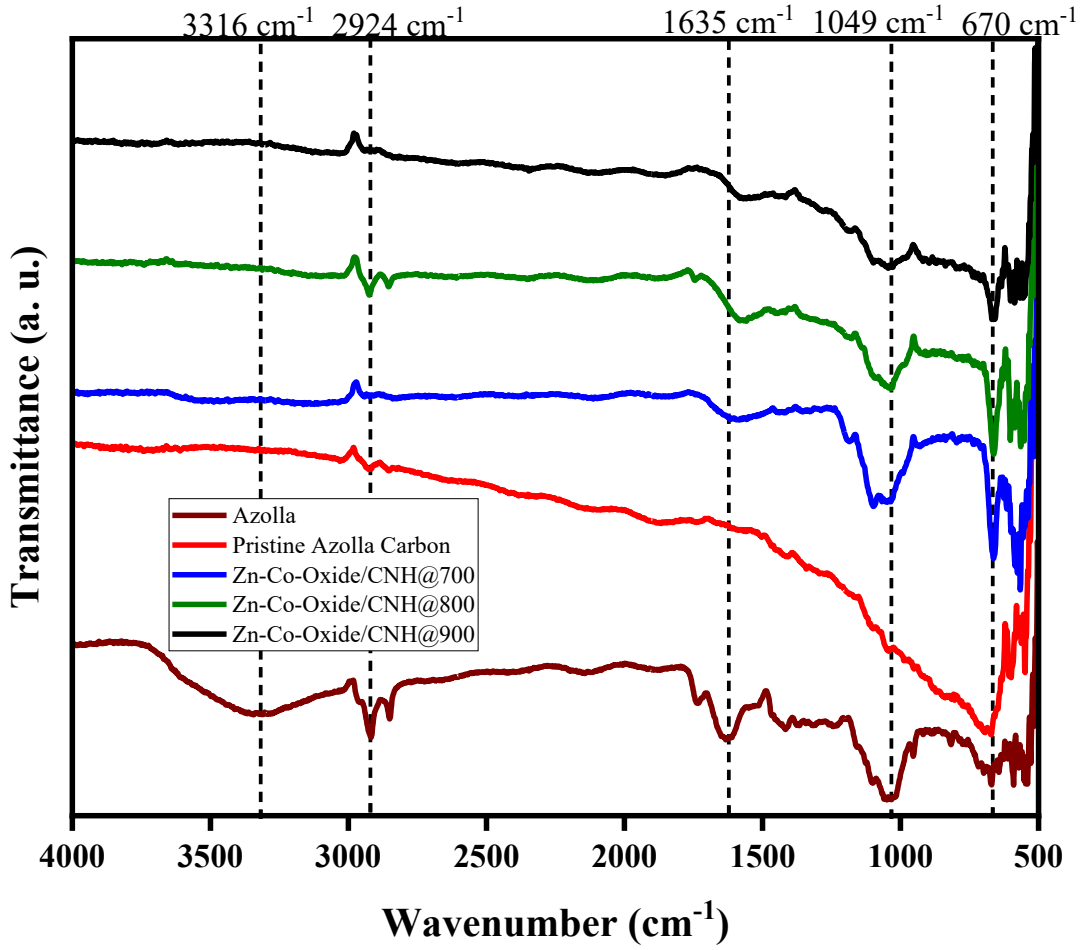

Figure 8: FTIR spectra of Azolla and Azolla-derived carbon

The FTIR spectra for all the metal incorporated carbon materials reveal the presence of N-doped graphitic carbon and the metal-ligand interactions. The peak at around 1635 cm^{-1} corresponds to C=C stretching vibration of the graphitic structure, which shows that the carbonization temperature of 700 °C to 900 °C leads to increased graphitization. The band around 1049 cm^{-1} is attributed to C-O stretching vibrations, indicating the existence of oxygen containing groups. The peak at 670 cm^{-1} is attributed to metal-oxygen (Zn-O and Co-O) vibrations, which helps to confirm the successful incorporation of the metal species into the carbon matrix. The gradual drop in the intensity of the O-H and C-H peaks and the increase in the intensity of C=C and metal-O peaks with increase in temperature show the improvement of carbonization temperature has a positive effect on the graphitization and metal-N

coordination, whereas the low temperature preserves the presence of more organic functional groups on the surface (Lei et al., 2022).

4.3 FESEM analysis

The field emission scanning electron microscopy (FESEM) analysis was done to study the surface morphology and structural evolution of the synthesized Zn-Co-Oxide/CNH composites at different carbonization temperatures i.e. 700 °C, 800 °C and 900 °C along with the pristine azolla and MOF-incorporated uncarbonized samples.

Figure 9 represents the field emission scanning electron microscopy (FESEM) images of Pristine azolla and metal integrated azolla biomass. The image of pristine azolla contains comparatively smooth surface structure whereas metal integrated azolla biomass showed crystal structures of about 1 μm size along with rough surface. This supports the formation of metal integrated biomass.

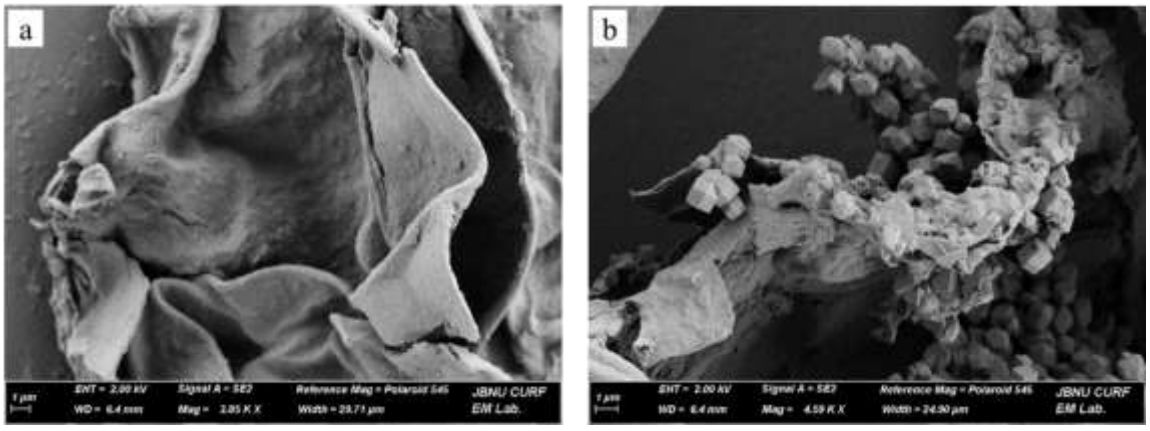

Figure 9: FESEM image of a) Pristine Azolla, b) Bimetallic MOF incorporated Azolla

Figure 10 represents the FESEM images of the as-prepared sample carbonized in 700 °C. Upon carbonization, significant morphological transformations are seen in all samples. The Zn-Co-Oxide/CNH shows highly aggregated and irregular structures with the formation of rough and porous carbon frameworks. It contains clustered particles suggesting partial decomposition of organic components and formation of carbonaceous structures. However, the pore distribution appears to be non-uniform. This may limit the efficient mass transfer during dye degradation.

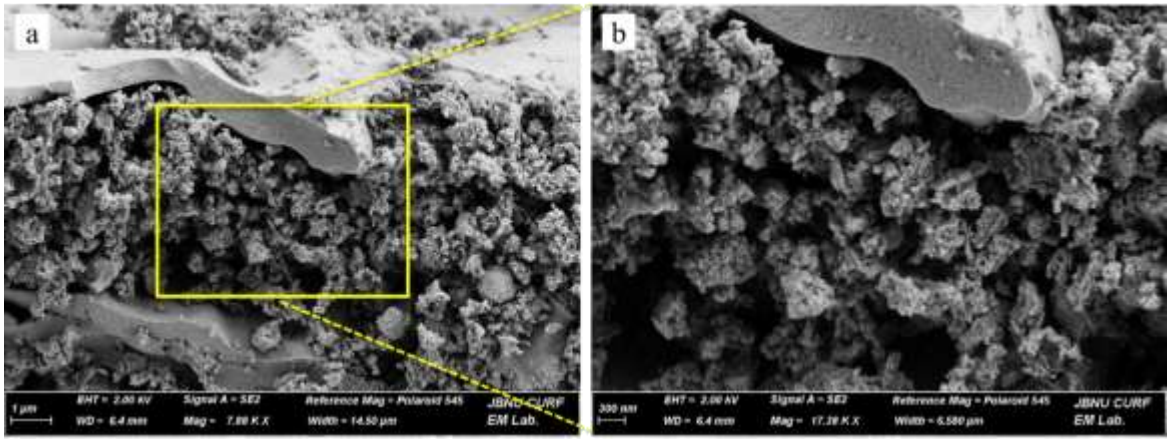

Figure 10: FESEM images of Zn-Co-Oxide/CNH@700

The Zn-Co-Oxide/CNH@800 becomes more defined than the sample carbonized at 700 °C as presented in **figure 11**. Interconnected porous networks are appeared with increased surface roughness. There is presence of partially developed spherical and irregular particles indicating the formation of metal oxide nanoparticles embedded within the carbon matrix. It supports the availability of active sites for the catalytic degradation.

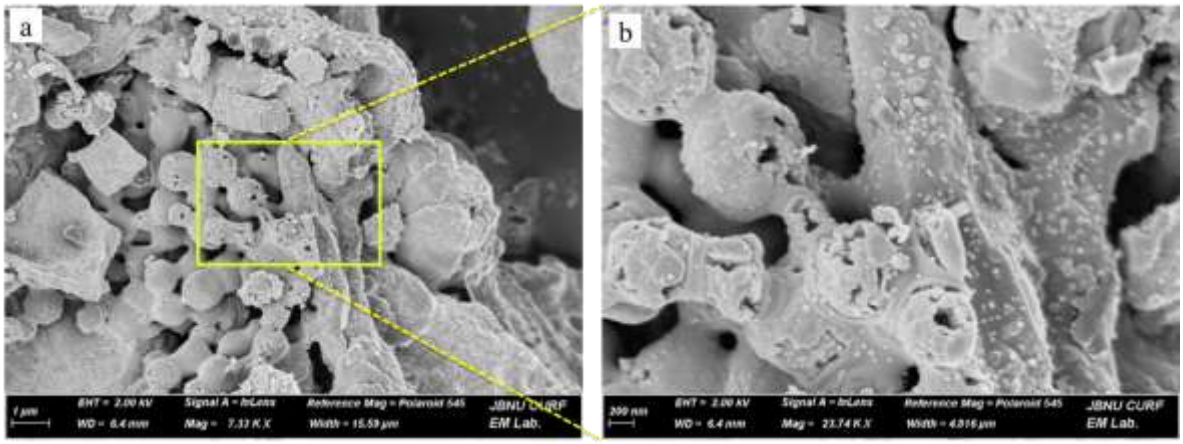

Figure 11: FESEM images of Zn-Co-Oxide/CNH@800

The Zn-Co-Oxide/CNH@900 exhibits a distinctly different surface morphology characterized by well-defined spherical and quasi-spherical particles as shown in **figure 12**. They are relatively uniform size distribution with approximately 400 nm diameter. These particles are so tightly packed but with inter-connecting voids that a highly porous structure is formed. This morphological structure formation can be explained by the higher level of decomposition of

the metal-organic frameworks precursor and the improved crystallization of the metal oxides at high temperature.

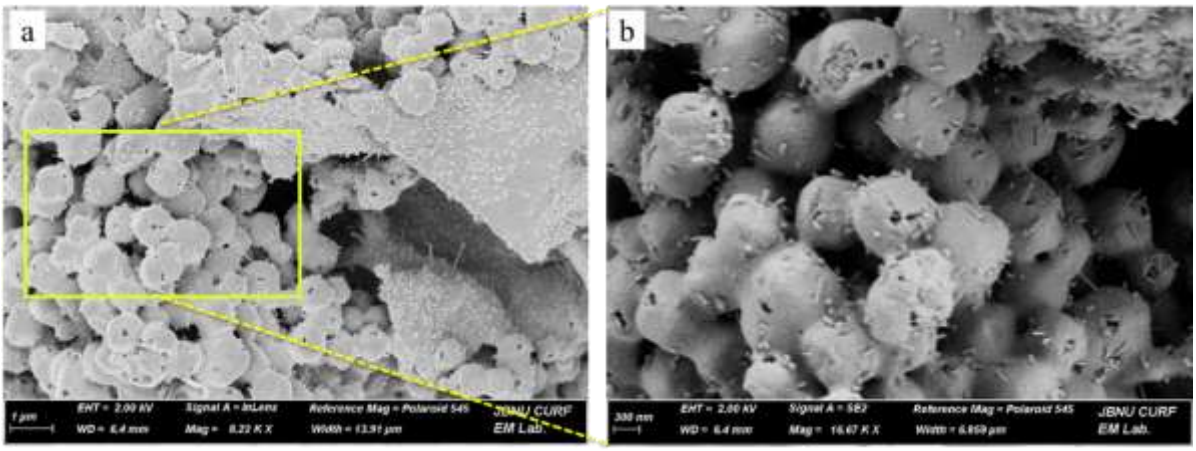

Figure 12: FESEM images of Zn-Co-Oxide/CNH@900

Comparatively, the progression from 700 °C to 900 °C clearly shows the effect of carbonization temperature on structural evolution. Higher the temperature, better the graphitization, improved pore development and more uniform dispersion of metal oxide nanoparticles.

4.4 EDX analysis

Figure 13 represents elemental mapping of the optimized Zn-Co-Oxide/CNH@900 sample using energy-dispersive X-ray spectroscopy (EDX). The elemental composition presents that carbon (C) is the dominant element with an atomic percentage of 65.64%. It confirms that the composite primarily consists of a carbonaceous matrix which is derived from the azolla biomass. Along with carbon, the other elements detected are nitrogen (N), Oxygen(O), Cobalt (Co) and Zinc (Zn) with atomic percentage 1.21%, 21.75%, 10.55% and 0.85% respectively. The highest percent of carbon indicates the formation of well-developed carbonaceous material derived from azolla biomass. This high carbon content also indicates the formation of a well-developed conductive matrix.

The presence of 21.75% oxygen indicates the presence of oxygen-containing functional groups and metal oxides within the structure. Such oxygen species play an important role in facilitating

surface reactions and promoting the generation of reactive oxygen radical during photocatalytic degradation of methylene blue.

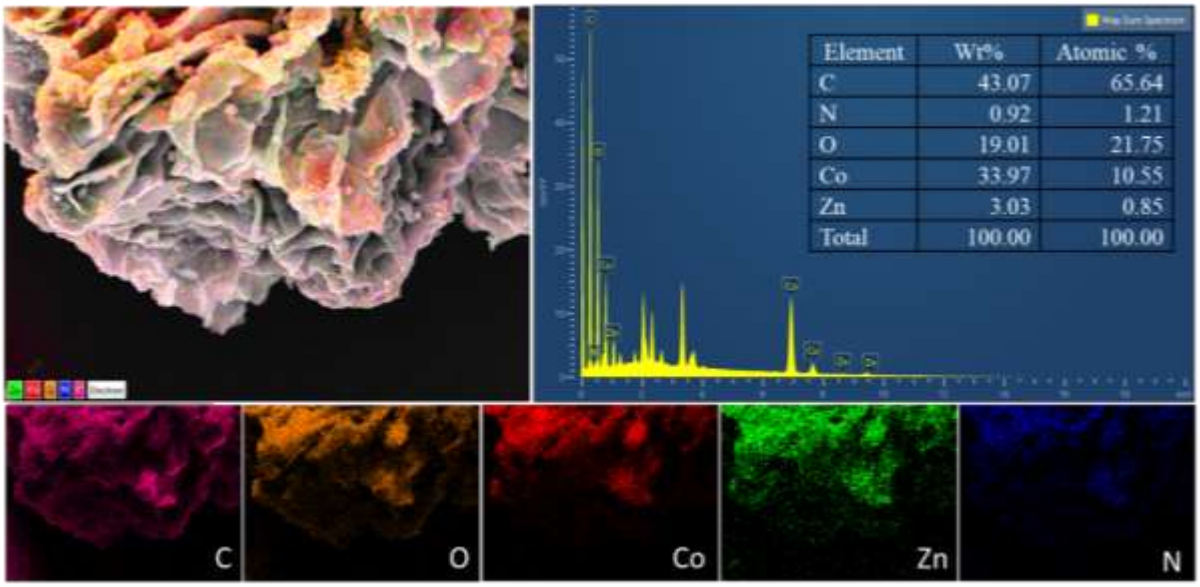

Figure 13: Elemental mapping of Zn-Co-Oxide/CNH@900

Cobalt (Co) shows 10.35% atomic percentage. It confirms the successful incorporation of cobalt species into the carbon matrix of azolla. It is particularly important as it serves as an active catalytic center and it enhances electron transfer processes improving photocatalytic efficiency. Comparative to cobalt, the amount of zinc is very low i.e. 0.85% only as the initial incorporation of zinc source was also least. The presence of both the metals confirms the formation of a bimetallic system. The lower content of zinc may also be attributed to partial loss or redistribution during high-temperature carbonization.

A small amount of nitrogen (1.21%) is also detected, originating from the biomass precursor or MOF ligand 2-methyl imidazole. Nitrogen doping is beneficial as it is known to modify the electronic structure of carbon, improve conductivity, and enhance adsorption interactions with dye molecules (Lin et al., 2023).

4.5 Photocatalytic degradation of methylene blue

UV-Vis absorption analysis

For the analysis of performance by as-prepared samples, photocatalytic degradation was done by taking 10 ppm methylene blue was a dye model. The methylene blue solution was magnetically stirrred for 120 minutes under uv irradiation. **Figure 14** depicts the UV-Vis spectra of photocatalytic MB degradation using different as-prepared sample. The pristine azolla-derived carbon performed limited photocatalytic degradation with 33% MB degradation within 120 minutes of UV irradiation. These carbon materials have some surface functional groups and a bit of porosity, which helps in dye adsorption. However, on their own, they do not show strong photocatalytic activity because they lack semiconductor components.

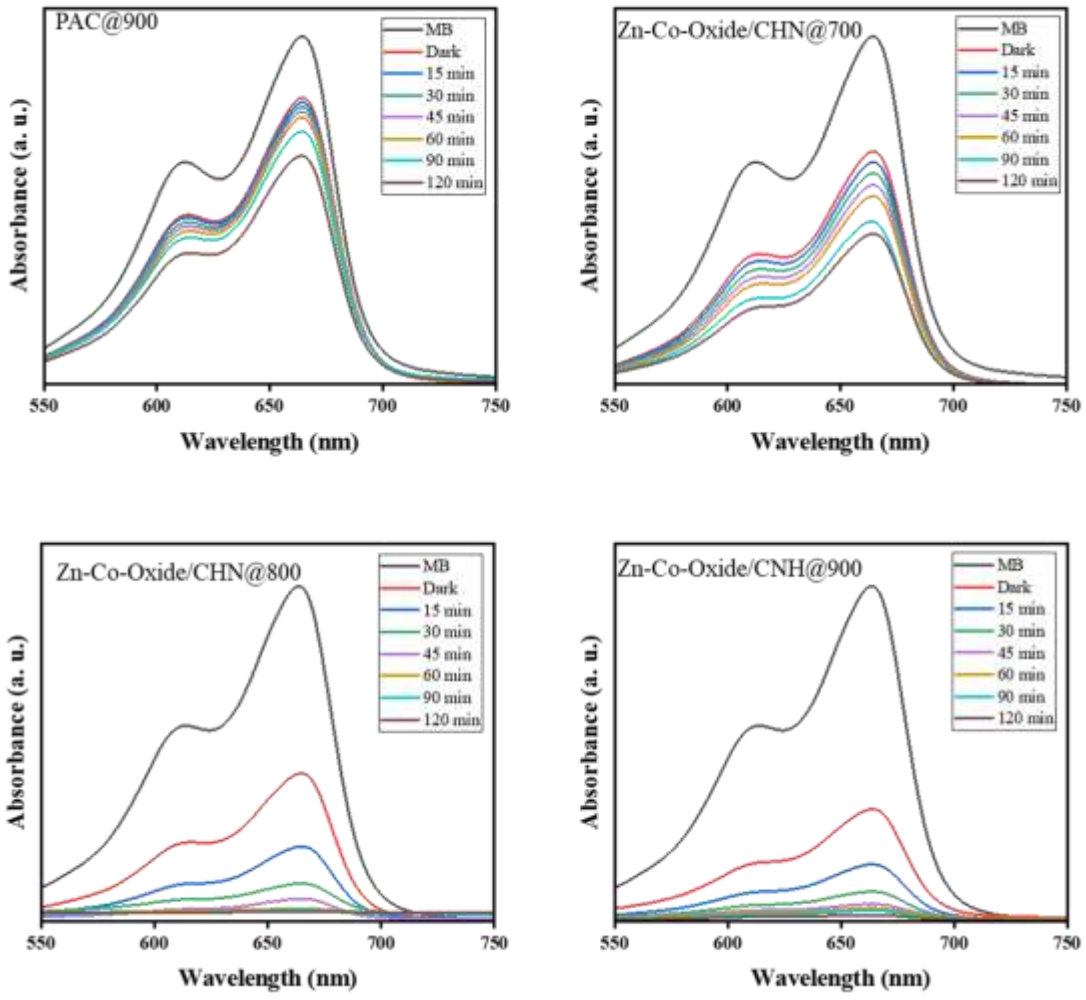

Figure 14: UV spectra of methylene blue after degradation using as-prepared sample

In contrast, the zinc-cobalt integrated azolla biomass-derived carbon (Zn-Co-Oxide/CNH@700, Zn-Co-Oxide/CNH@800, and Zn-Co-Oxide/CNH@900) showed a enhancement in degradation efficiency. Zn-Co-Oxide/CNH@700 resulted 54% degradation whereas Zn-Co /CH@800 and Zn-Co/CH@900 showed 92-93% removal of MB under identical conditions.

This clear improvement shows that the metal oxide particles were successfully added into the carbon during carbonization and calcination. When the light is on ZnO cooperates with cobalt

oxide as a photocatalyst to create electron-hole pairs that participate in reactions to generate hydroxyl and superoxide radicals as presented in **figure 15**. These species degrade the structure of the methylene blue, resulting in the degradation of methylene blue.

Furthermore, the existence of both ZnO and cobalt oxide can generate a heterojunction for effective charge separation and decrease the electron-hole recombination. This results in an overall better photocatalytic performance.

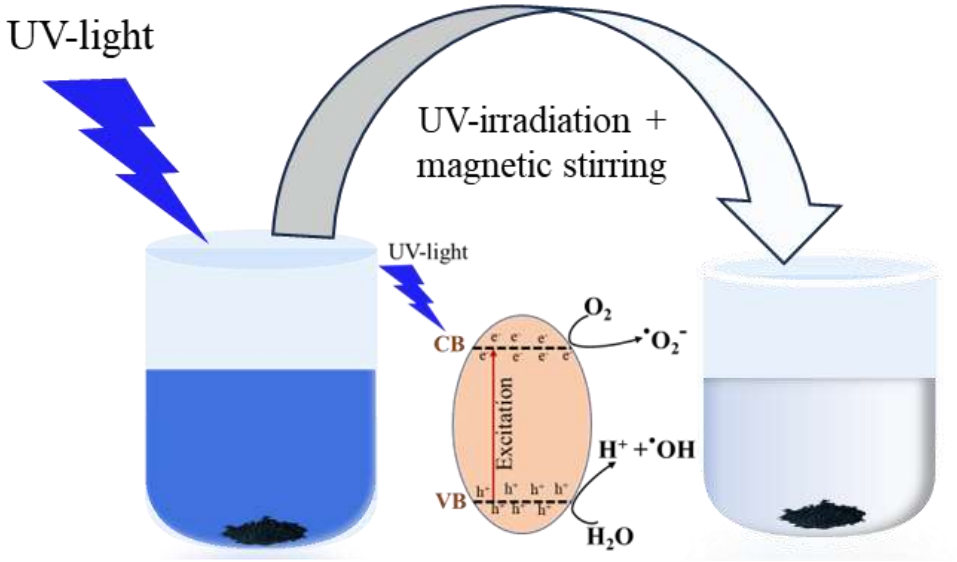

Figure 15: Schematic diagram of MB degradation under UV irradiation while magnetic stirring

The degradation process is enhanced by the use of the carbon obtained from the azolla, which allows for better charge transfer as an electron carrier. It also has a large surface area to attach through π-π interaction of methylene blue (MB) molecule. This brings the pollutant into contact with the active sites, and renders the degradation process more rapid.

In conclusion, the degradation efficiency of the MOF-derived composites is over 90%, which is about three times higher than that of pristine carbon at 33%, indicating the strong effect of the metal oxides incorporated into the MOF and the synergistic effect of the carbon matrix and semiconductor phases. Therefore, the developed MOF-derived bimetallic carbon composites represent highly effective and promising materials for the photocatalytic treatment of dye.

The degradation behavior of Methylene Blue over time was evaluated by plotting the normalized concentration (C/C_0) as a function of irradiation time, which provides a clear visualization of the progressive decrease in dye concentration during the photocatalytic process as presented in **figure 16**. First, the samples were kept in the dark for 30 minutes to reach adsorption equlibrium, and then UV light was applied up to next 120 minutes to study photocatalytic degradation. This helps to separate how much removal is due to adsorption and how much is due to photocatalysis.

During the dark period upto 30 min, all samples showed some removal due to adsorption. Zn-Co-Oxide/CNH@900 showed the highest adsorption (C/C_0 = 0.370), followed by Zn-Co-Oxide/CNH@800 (0.471). Zn-Co/CH@700 showed lesser adsorption (0.686), and pristine azolla carbon showed the least change i.e. 0.833. After the irradiation of UV-light, Zn-Co-Oxide/CNH@800 and Zn-Co-Oxide/CNH@900 showed fast degradation. Zn-Co-Oxide/CNH@900 decreased to about 0.070 at 120 minutes, and Zn-Co-Oxide/CNH@800 also showed a similar result (0.081). The difference between them is very small. This performance suggests that 800 °C is already enough, and increasing to 900 °C does not improve much. Zn-Co/CNH@700 also showed degradation under UV, but it was much lower. It reached around 0.462 at 120 minutes. This lower performance may be due to less development of active sites and lower graphitization at 700 °C.

Pristine azolla carbon showed very little photocatalytic activity comparatively. The value only decreased slightly from 0.833 to about 0.674 after 120 minutes (i.e. 33% removal). This shows that carbon alone is not very effective, and the main role in photocatalytic degradation is due to the Zn-Co-oxide components formed on the carbon matrix.

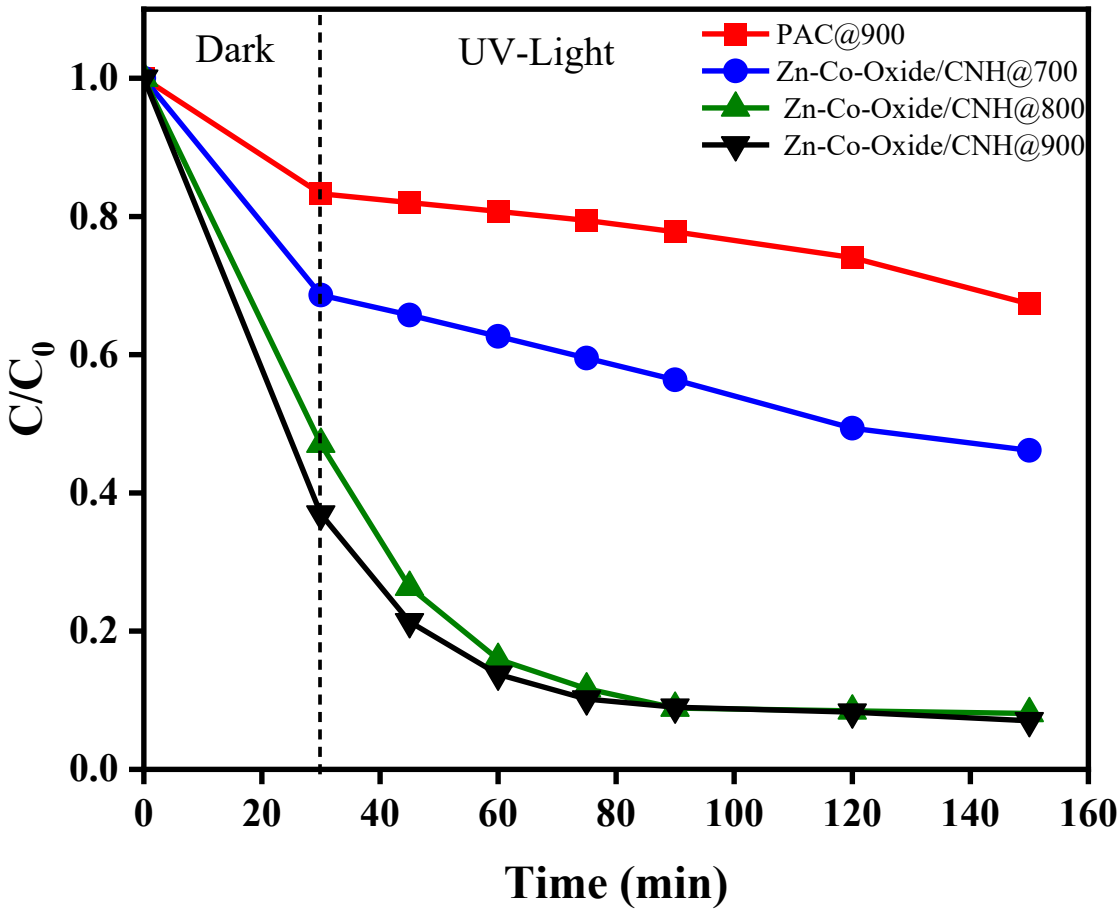

Figure 16: Effect of catalyst dose on the photocatalytic degradation of 10 ppm MB

The **figure 17** also supports the confirmation of methylene blue degradation by more than 90% frpm the fading colour change observed in increasing time of UV irradiation.

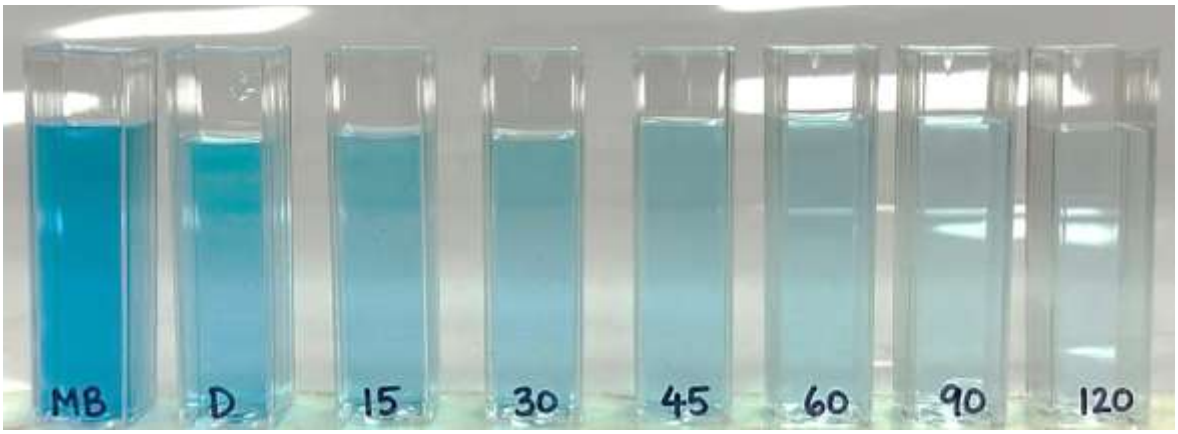

Figure 17: Colour changes of methylene blue over time

Figure 18 also shows the clear % degradation increasing from sample PAC@900 to Zn-Co-Oxide/CNH@900. It shows that even in the dark, Zn-Co-Oxide/CNH@900 shows about 63% degradation which indicates strong adsorption capacity before any UV irradiation. Upon UV exposure, both Zn-Co-Oxide/CNH@800 and Zn-Co-Oxide/CNH@900 rapidly reach above 85-90% degradation within 45 minutes, demonstrating excellent photocatalytic efficiency. Zn-Co-Oxide/CNH@700 shows moderate performance, while PAC@900 remains the weakest performer, likely acting mainly as an adsorbent. Overall, the results highlight that Zn-Co-Oxide/CNH composites, especially those synthesized at higher temperatures, are highly effective photocatalysts for dye degradation.

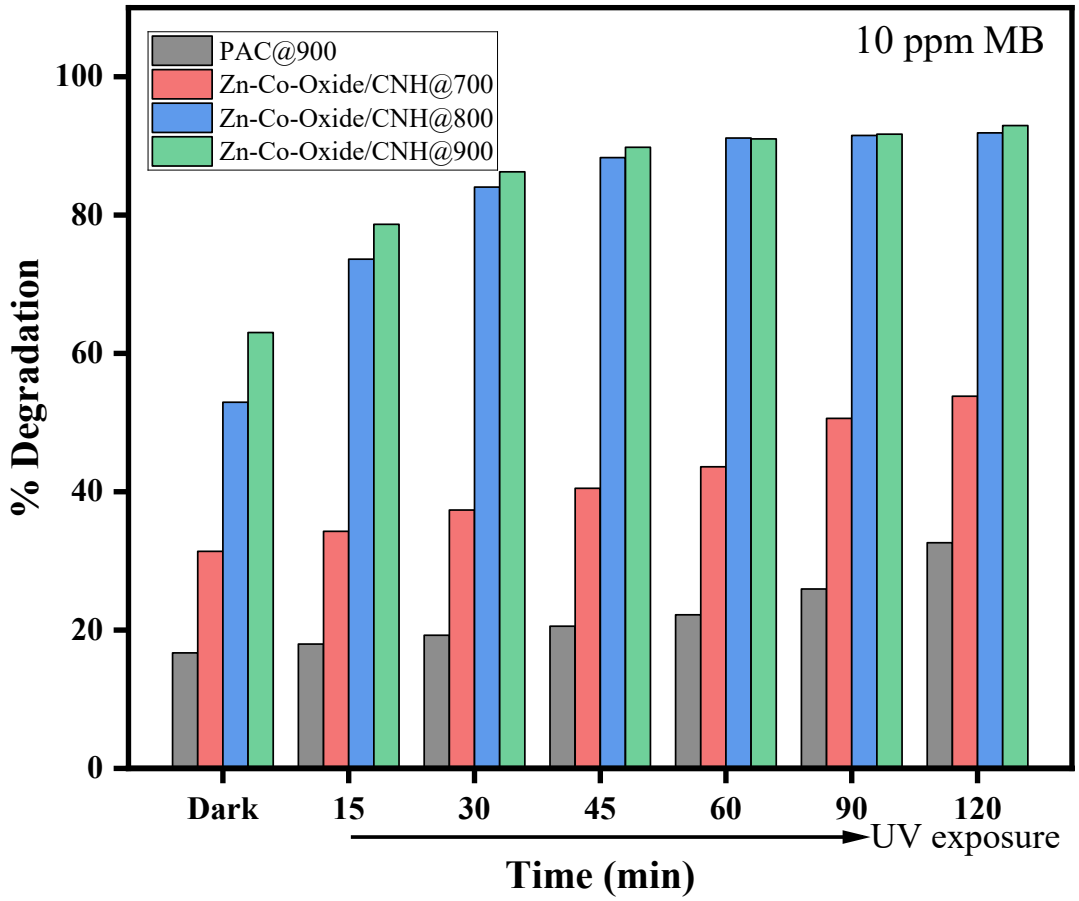

Figure 18: MB degradation (%) over different samples at 10 ppm, including dark adsorption and UV irradiation up to 120 min

4.6 Adsorption isotherm studies

Adsorption isotherm studies were performed to understand the interaction between the methylene blue molecules and the surface of the as-prepared carbon samples, as well as to determine the maximum adsorption capacity along with the nature of the adsorption process. Two isotherm models were used to analyze the equilibrium adsorption data namely Langmuir isotherm and Freundlich isotherm. These models were analyzed to all the four sample: PAC@900, Zn-Co-Oxide/CNH@700, Zn-Co-Oxide/CNH@800 and Zn-Co-Oxide/CNH@900.

I. Langmuir isotherm

The Langmuir isotherm model assumes that the adsorption occurs on a uniform surface with finite number of identical adsorption sites. It assumes that all adsorption sites have equal energy and there is no interaction between adsorbed molecules (Azizian et al., 2018).

The equilibrium adsorption capacity (q_e) was calculated by using the mass balance equation (Devi & Tyagi, 2022):

$$q_e = \frac{(C_0 - C_e)V}{m} \quad [3]$$

Where, C_0 = Initial concentration of MB solution (mg. L^{-1})

C_e = Equilibrium concentration of MB solution (mg. L^{-1})

V = Volume of the solution (L)

M = Mass of adsorbent (g)

The Langmuir equation can be written as follows in its linear form:

$$\frac{c_e}{q_e} = \frac{1}{k_L q_{\max}} + \frac{c_e}{q_{\max}} \quad [4]$$

Where q_{max} (mg/g) depicts the maximum adsorption capacity corresponding to complete monolayer coverage, K_L (L/mg) is the Langmuir constant related to the affinity of the binding sites. The plot C_e/q_e versus C_e gives a straight line where slope is equal to $1/q_{max}$ and intercept equal to $1/(q_{max}K_L)$.

The Langmuir isotherm plots for all four samples are presented in **figure 19**, and the calculated parameters are summarized in **table 2**. It is observed that R^2 values for PAC@700 and Zn-Co-Oxide/CNH@700 were very low, i.e. 0.0697 and 0.237 respectively. It indicates that the Langmuir model does not describe the adsorption behavior adequately of these two samples. This poor fit also suggests that these two samples does not follow uniform monolayer adsorption mechanism. In contrast, the remaining two samples Zn-Co-Oxide/CNH@800 and Zn-Co-Oxide/CNH@900 showed significantly higher R^2 values of 0.9645 and 0.9827

respectively. It indicates a good Langmuir model fit for these samples. The maximum monolayer adsorption (q_{max}) was calculated to be 97.47 mg/g for Zn-Co-Oxide/CNH@800 whereas it was 99.7 mg/g for Zn-Co-Oxide/CNH@900. Since the fit is poor in PAC@900 and Zn-Co-Oxide/CNH@700, the value of q_{max} cannot be interpreted. The value of K_L were 0.15 L/mg and 0.20 l/mg for Zn-Co-Oxide/CNH@800 and Zn-Co-Oxide/CNH@900 respectively. It suggests that these samples are relatively favorable and moderately strong interaction between MB molecules and the sample surface.

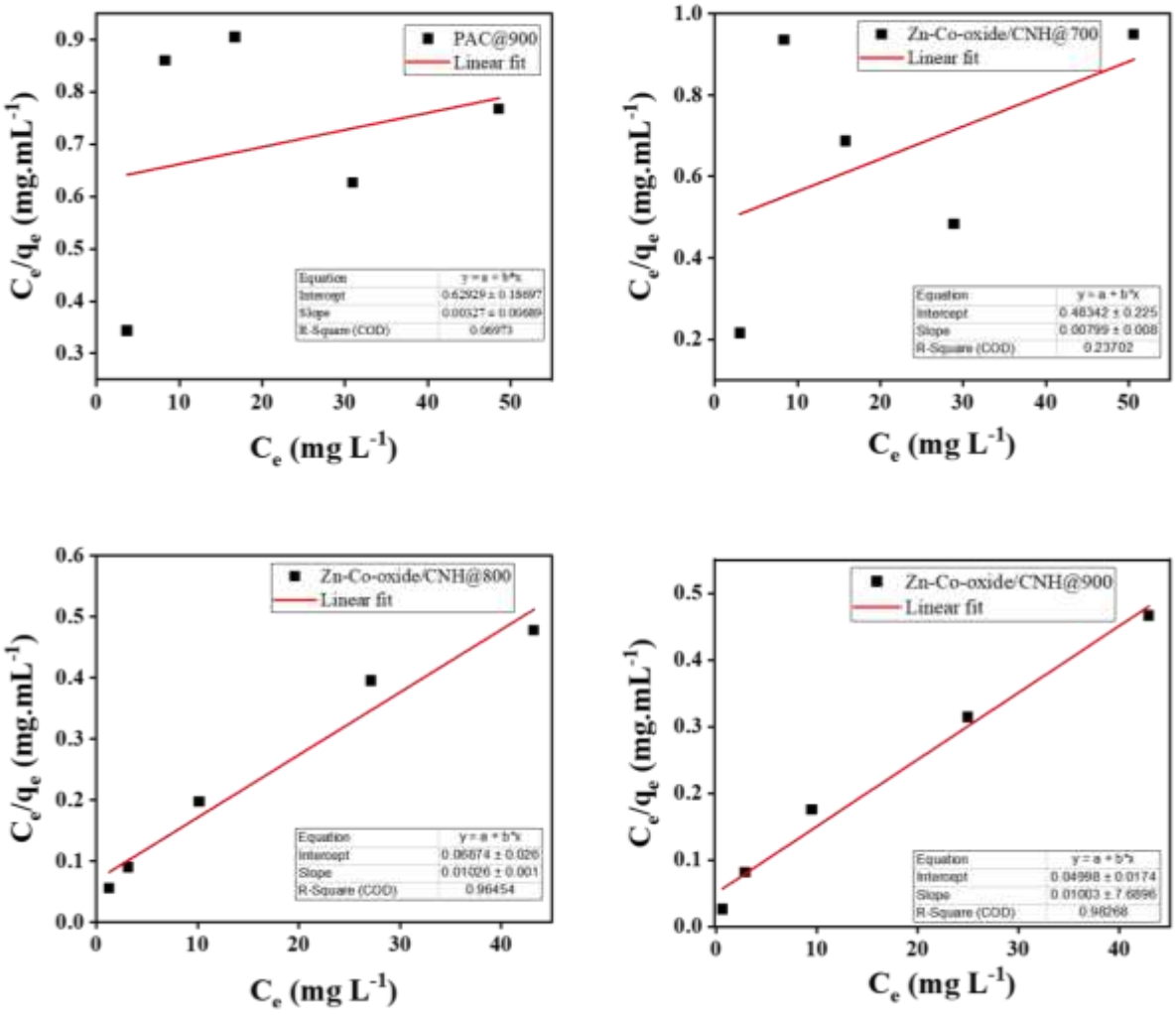

Figure 19: Langmuir isotherm fit of four different carbon samples varying concentration of MB

Table 2: Parameters of Langmuir isotherm model

Sample	**Slope**	**Intercept**	**q_{max} (mg/g)**	**K_L (L/mg)**	**R^2**
PAC@900	0.0033	0.62929	305.81	0.01	0.0697
Zn-Co-Oxide/CNH@700	0.008	0.48342	125.16	0.02	0.237
Zn-Co-Oxide/CNH@800	0.0103	0.06874	97.47	0.15	0.9645
Zn-Co-Oxide/CNH@900	0.01	0.04998	99.70	0.20	0.9827

II. Freundlich isotherm

The Freundlich isotherm describes adsorption on heterogenous surfaces with non-uniform distribution of adsorption energies. It also assumes that the adsorption capacity increases with dye concentration (Vigdorowitsch et al., 2021). This model does not assume monolayer coverage but account for multilayer adsorption. The linear form of Freundlich isotherm equation is expressed as:

$$\log q_e = \log K_F + \frac{1}{n} \log C_e \qquad [5]$$

Where q_e (mg/g) is the equilibrium capacity, C_e (mg/L) is the equilibrium concentration of dye in solution, K_F is the Freundlich constant and n is the heterogeneity factor that indicates the adsorption intensity (Foo & Hameed, 2010).

From the plot of log q_e versus log C_e, a straight line with slope equal to 1/n and intercept equal to log K_F can be obtained. The value of 1/n less than 1 indicates favorable adsorption and a heterogenous surface whereas the value greater than 1 indicates cooperative adsorption (Crini & Badot, 2008). The plots of Freundlich isotherm are presented in **figure 20** and its derived parameters are presented in **table 3**. The results showed that the Freundlich model is better fit for Zn-Co-Oxide/CNH@800 and Zn-Co-Oxide/CNH@900 as R^2 values are 0.9912 and 0.9892

respectively, which are even slightly greater than that obtained from the Langmuir model. This suggests that though the Langmuir model fits well for the same 2 samples, the Freundlich model describes their adsorption behavior equally well and even slightly better. It suggests a degree of surface heterogeneity in the composite materials. The value of Freundlich capacity constant (K_F) was 21.89 and 27.86 for Zn-Co-Oxide/CNH@800 and Zn-Co-Oxide/CNH@900 respectively, which are significantly higher than those of PAC@900 (2.74) and Zn-Co-Oxide/CNH@700 (4.71). It confirms the better adsorption capacity of the as-prepared composite materials carbonized at higher temperatures.

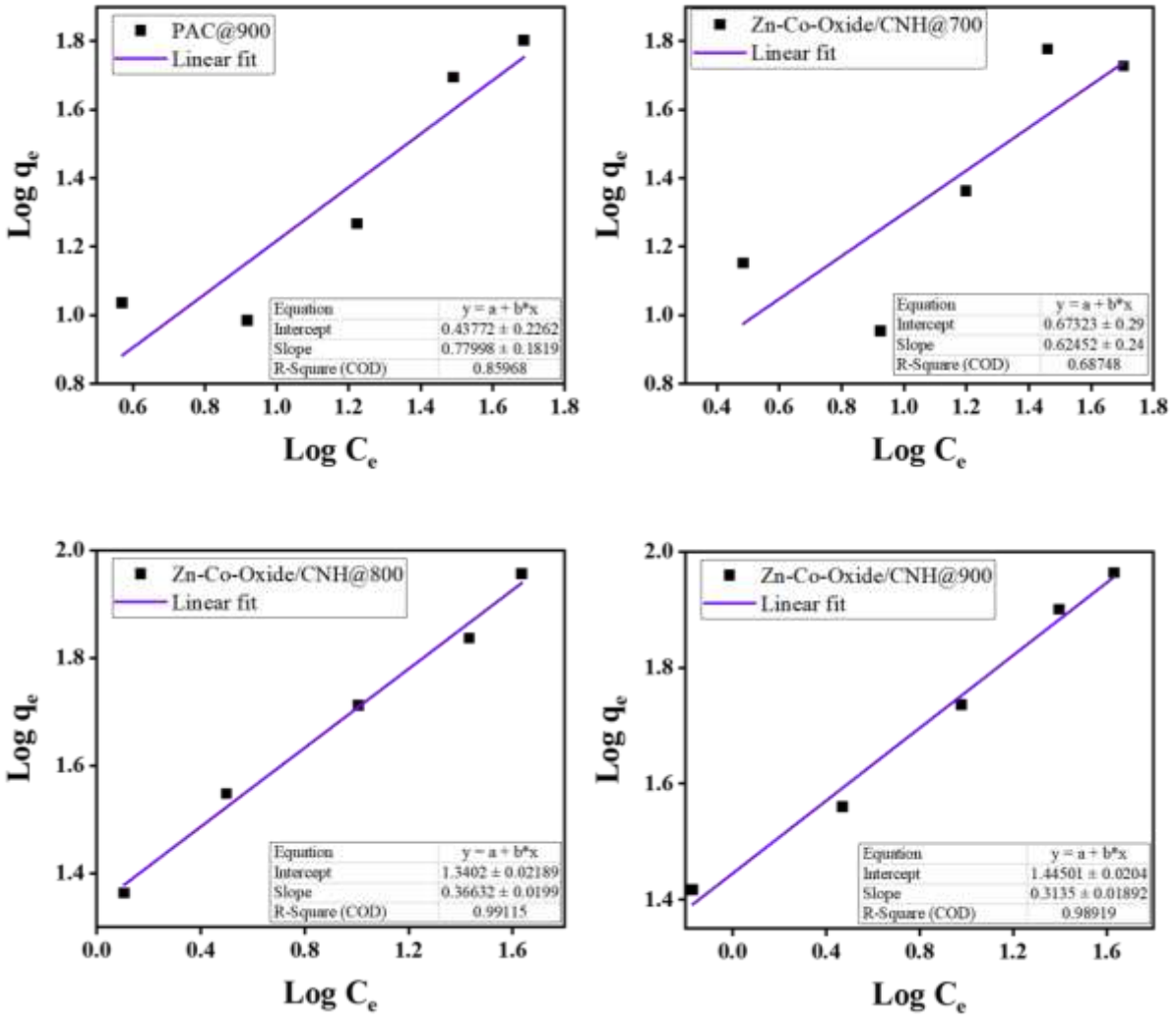

Figure 20: Freundlich isotherm fit of four different carbon samples varying concentration of MB

Table 3: Parameters of Freundlich isotherm model

Sample	**Slope**	**Intercept**	**K_F**	**n**	**R^2**
PAC@900	0.78	0.43772	2.74	1.28	0.8597
Zn-Co-Oxide/CNH@700	0.6245	0.67323	4.71	1.60	0.6875
Zn-Co-Oxide/CNH@800	0.3663	1.3402	21.89	2.73	0.9912
Zn-Co-Oxide/CNH@900	0.3135	1.44501	27.86	3.19	0.9892

The 1/n values (slope) obtained for all samples were less than 1 as depicted in **table 3**. It confirms favorable adsorption conditions and indicates a heterogenous adsorption surface for all synthesized materials (Foo & Hameed, 2010). The gradual decrease in 1/n values from PAC@900 to Zn-Co-Oxide/CNH@900 suggests increasing surface heterogeneity and stronger adsorption affinity in the composites.

Comparing the two isotherm models for all the samples, it has shown that both the Langmuir and Freundlich isotherm model fits for Zn-Co-Oxide/CNH@800 and Zn-Co-Oxide/CNH@900 whereas it poorly fits in case of PAC@900 and Zn-Co-Oxide/CNH@700. This result of PAC@900 and Zn-Co-Oxide/CNH@700 suggests that the adsorption of MB onto the synthesized materials does not strictly follow either a homogenous monolayer or a simple heterogenous multilayer mechanism. It might be due to the irregular surface properties of these materials. In contrast, the fitting of Zn-Co-Oxide/CNH@800 and Zn-Co-Oxide/CNH@900 indicates well-defined and consistent adsorption behavior.

4.7 Photocatalytic degradation kinetics

To study the kinetic behavior of photocatalytic degradation of MB, the experimented data were fitted into two kinetic models: pseudo-first-order (PFO) and pseudo second order (PSO) kinetic models.

I. Pseudo-First-Order Kinetic Model

Pseudo first order kinetic model is also known as the Langmuir-Hinshelwood model. It is usually applied to describe photocatalytic degradation of organic dyes in aqueous solution (Konstantinou & Albanis, 2004) It assumes that the rate of degradation is directly proportional to the concentration of the dye remaining in the aqueous solution at any given time. The linear form of PFO equation is expressed as:

$$\ln\left(\frac{C_0}{C_t}\right) = k_1 \cdot t \qquad [6]$$

Where, C_0 (mg/L) is the initial dye concentration, C_t is the dye concentration at time t, k_1 (min^{-1}) is PFO rate constant and t is the irradiation time (Chong et al., 2010). A plot of $\ln(C_0/C_t)$ versus time gives a straight line passing through the origin, with the slope equal to the rate constant.

The pseudo-first-order kinetic plots for all four samples are presented in **figure 21,** and the calculated rate constants along with their corresponding R^2 values are summarized in **table 4**. The results show that PAC@900 and Zn-Co-Oxide/CNH@700 exhibited good linearity with R^2 values of 0.946 and 0.993 respectively, indicating that the photocatalytic degradation of methylene blue over these two materials follows the pseudo-first-order kinetic model well. The rate constant k_1 for Zn-Co-Oxide/CNH@700 was found to be 0.00346 min^{-1}, which is approximately twice that of PAC@900 (0.00169 min^{-1}), suggesting a faster degradation rate for the composite material compared to plain activated carbon. However, the Zn-Co-Oxide/CNH@800 and Zn-Co-Oxide/CNH@900 samples showed relatively lower R^2 values of 0.762 and 0.791 respectively under the pseudo-first-order model, indicating that this model does not describe the degradation kinetics well for these two higher-temperature composite materials despite their higher rate constants of 0.01376 min^{-1} and 0.01248 min^{-1}.

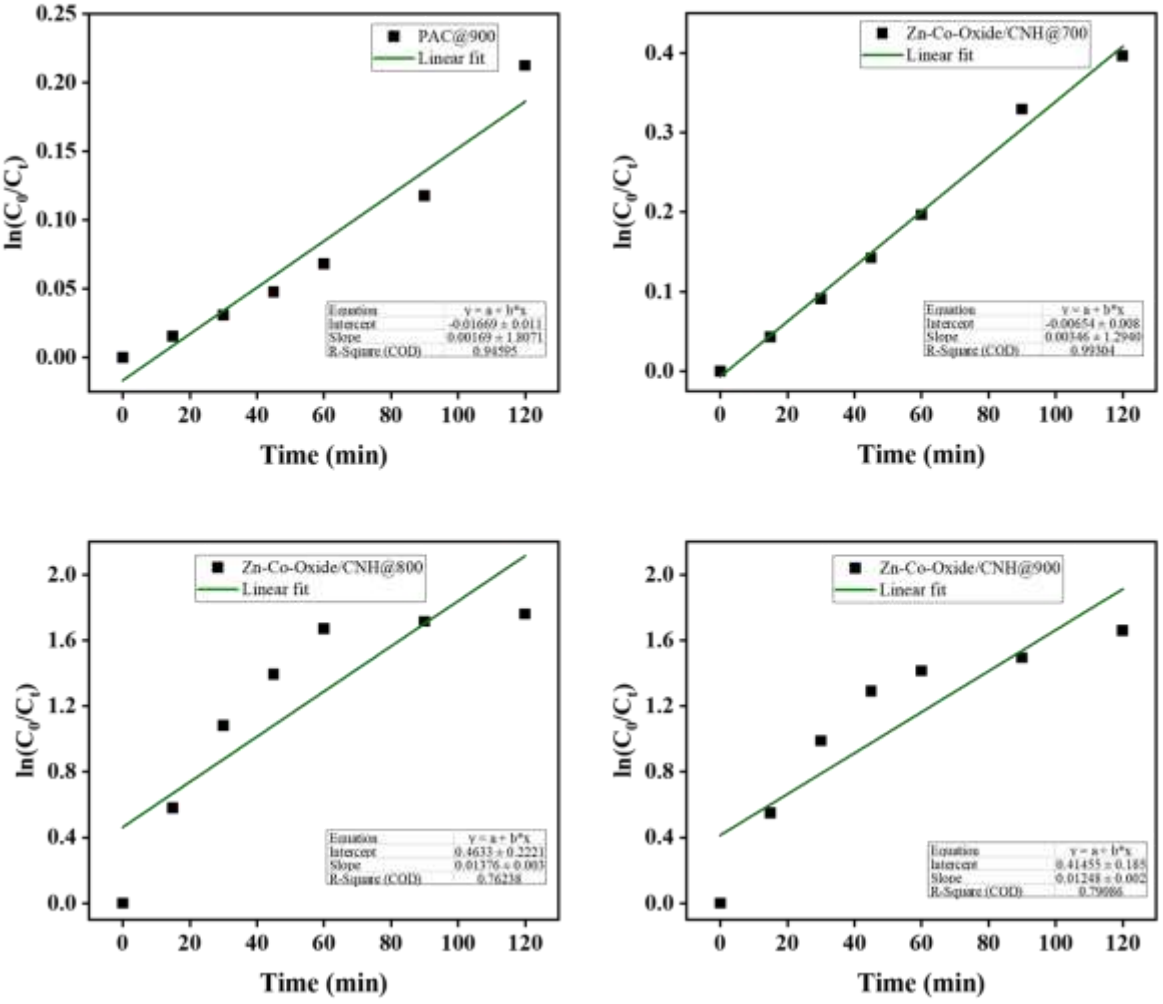

Figure 21: Pseudo-First-Order photocatalytic kinetics varying time

The poor fit of the pseudo-first-order model for Zn-Co-Oxide/CNH@800 and Zn-Co-Oxide/CNH@900 suggests that their degradation mechanism is more complex and cannot be simply described by a concentration-dependent linear relationship alone. As clearly shown in the bar chart (**figure 22**), Zn-Co-Oxide/CNH@800 exhibited the highest rate constant among all samples, followed closely by Zn-Co-Oxide/CNH@900, confirming that higher carbonization temperatures produce composite materials with significantly enhanced photocatalytic activity.

Table 4: R^2 values of as-prepared samples obtained from PFO kinetic model

Sample	Rate Constant (k) (min^{-1})	R^2
PAC@900	0.00169	0.946
Zn-Co-Oxide/CNH@700	0.00346	0.993
Zn-Co-Oxide/CNH@800	0.01376	0.762
Zn-Co-Oxide/CNH@900	0.01248	0.791

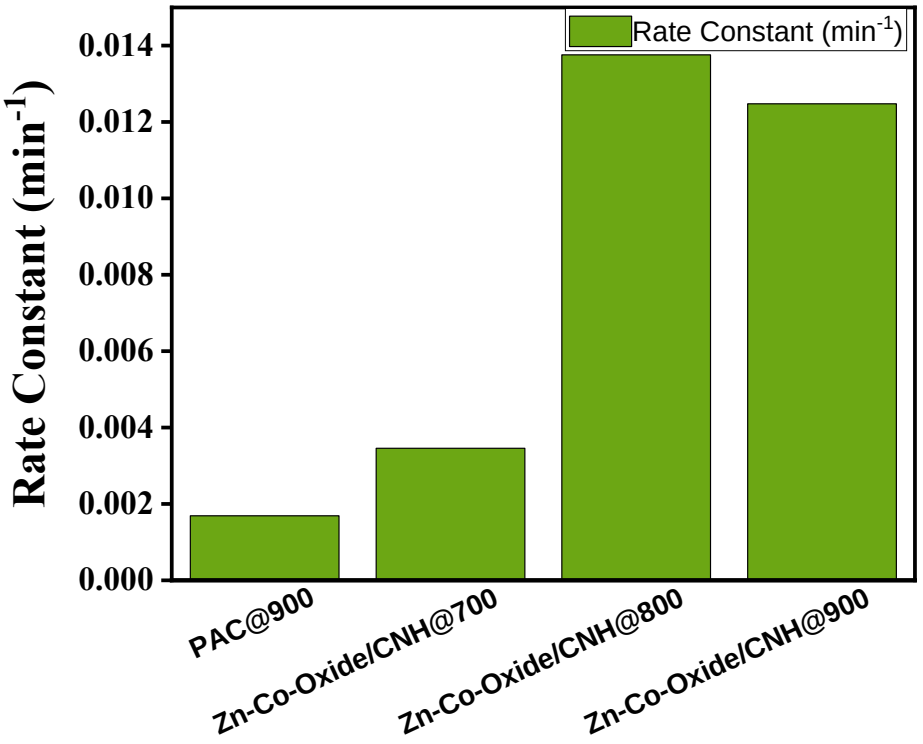

Figure 22: Bar chart showing PFO ate constant values of as-prepared samples

II. Pseudo-Second-Order Kinetic Model

The pseudo-second-order kinetic model assumes that the rate of degradation is proportional to the square of the remaining dye concentration and that chemisorption or surface reaction is the rate-limiting step in the overall degradation process (Ho & McKay, 1999). The linear form of the pseudo-second-order equation is expressed as:

$$\frac{1}{C_t} = k_2 + \frac{1}{C_o} \qquad [7]$$

where k_2 (L mg^{-1} min^{-1}) is the pseudo-second-order rate constant, and t (min) is the irradiation time (Ho & McKay, 1999). A plot of $1/C_t$ versus time gives a straight line with slope equal to k_2 and intercept equal to $1/C_0$.

The pseudo second order kinetic plot of all four samples is shown in **figure 23** and the parameters derived are given in **table 5**. From the results, the model of pseudo-second order was found to be the best fit for the photocatalytic degradation of MB over all the samples as the highest R^2 value was obtained for Zn-Co-Oxide/CNH@700, which was nearly equal to 1.0. PAC@900 also showed a reasonably good fit with an R^2 value of 0.93134 and a slope of 2.62956×10^{-4} L mg^{-1} min^{-1}. The R^2 value of the pseudo-second-order model of the Zn-Co-Oxide/CNH@900 sample was 0.91733, which is a significant improvement compared to its pseudo-first-order model with an R^2 value of 0.791, indicating that the pseudo-second-order model is a more suitable model for describing the degradation kinetics of the sample. In the same way, the pseudo-second-order model provided an R^2 of 0.86384 for Zn-Co-Oxide/CNH, whereas the pseudo-first order model gave an R^2 of 0.762. The pseudo-second-order plots gave intercept values equal to $1/C_0$, and the intercepts obtained were 0.13762, 0.1671, 0.41645 and 0.48955 for the PAC@900, Zn-Co-Oxide/CNH@700, Zn-Co-Oxide/CNH@800 and Zn-Co-Oxide/CNH@900 respectively, which were corroborating with the initial dye concentrations used in the experiments.

Table 5: Parameters obtained from PSO photocatalytic kinetic model

Sample	R^2	K_2
PAC@900	0.93134	2.62956×10^{-4}
Zn-Co-Oxide/CNH@700	0.99002	7.24658×10^{-4}
Zn-Co-Oxide/CNH@800	0.86384	0.41645
Zn-Co-Oxide/CNH@900	0.91733	0.48955

Comparing the fitting results of the pseudo-first-order model and the pseudo-second-order model to the results for all of the samples, it is clear that the pseudo-first-order model is a better kinetic model to describe the degradation of PAC@900 and Zn-Co-Oxide/CNH@700, while the pseudo-second-order model is a better kinetic model to describe the degradation of Zn-Co-Oxide/CNH@800 and Zn-Co-Oxide/CNH@900. Based on the high temperature composites better fit to the pseudo-second-order model, this indicates that surface interaction and chemisorption-type mechanisms are more important in the degradation process of these materials, and this is attributed to the fact that they have more developed surface structures and higher density of active sites at higher carbonization temperatures. The calculated rate constants of the pseudo-first-order reaction model clearly indicate that the Zn-Co-Oxide/CNH composites prepared at 800 °C and 900 °C have much better photocatalytic activity than the PAC@900 and Zn-Co-Oxide/CNH@700, respectively, with the rate constant being in the order of 4 to 8 times higher. The enhancement of photocatalytic activity is due to the well-developed porous carbon structure, the high dispersion of Zn-Co oxide nanoparticles, the enhanced separation of charge carriers and the increased light harvesting capability of the composites prepared at higher temperatures (Zhang et al., 2026). Overall, the kinetic analysis shows that the Zn-Co-Oxide/CNH prepared at 800 °C and 900 °C are the most kinetically

active samples in the photocatalytic degradation of methylene blue among all the synthesized samples.

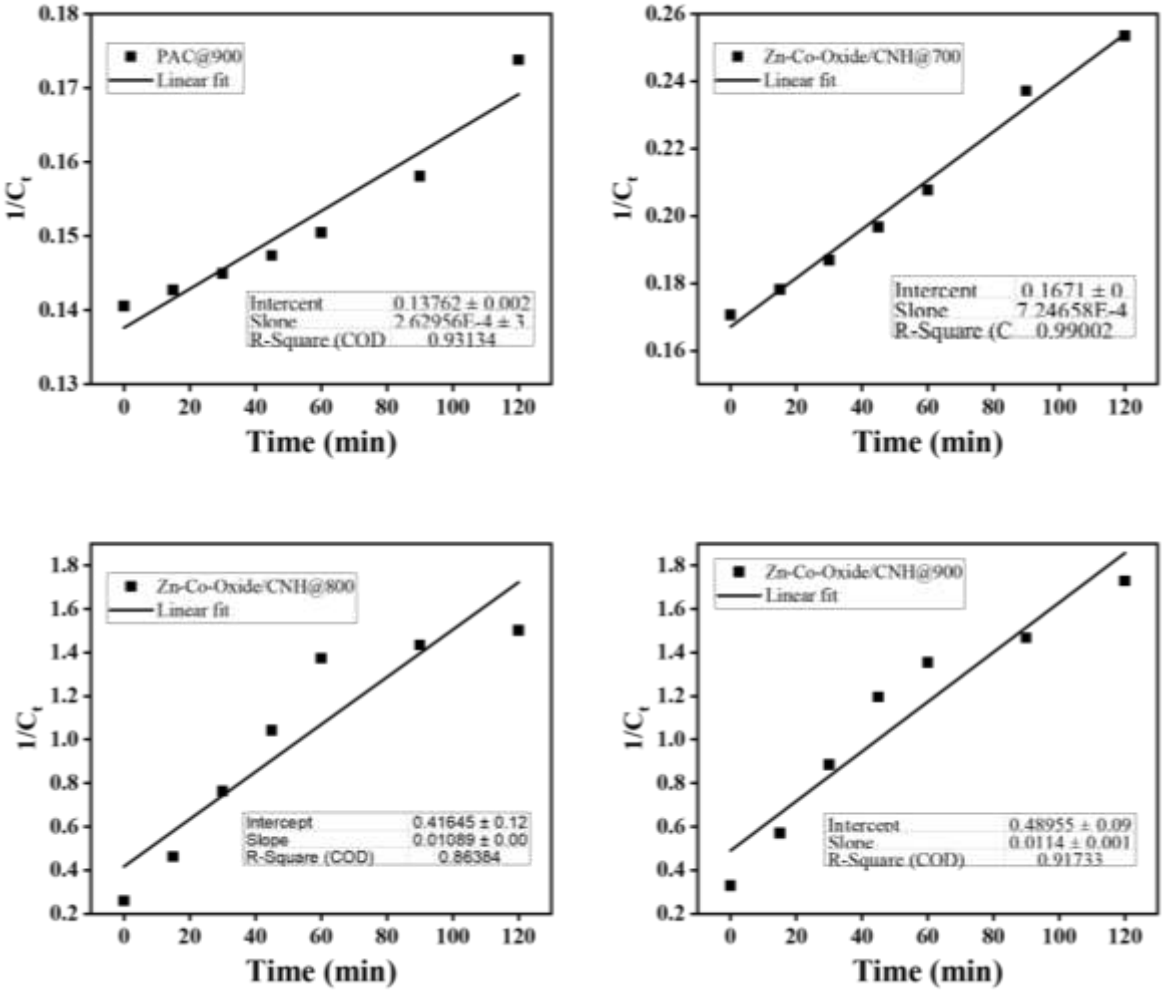

Figure 23: Pseudo-second-order photocatalytic kinetic model varying time

CHAPTER 5

5. Conclusions

Azolla biomass-derived carbon-based bimetallic metal-organic framework composites were successfully fabricated with carbonization temperature of 700 ℃, 800 ℃ and 900 ℃ and evaluated for methylene blue removal by adsorption and photocatalytic degradation. The XRD analysis showed that the Zn-Co oxide spinel phase was successfully formed inside the carbon matrix with crystallinity gradually increasing with an increase in the carbonization temperature. FESEM analysis revealed a highly porous and interconnected carbon framework in the higher-temperature samples, and EDX confirmed the successful incorporation of bimetallic active sites within the conductive carbon matrix.

Adsorption isotherm studies showed that Zn-Co-Oxide/CNH@800 and Zn-Co-Oxide/CNH@900 fitted well to both Langmuir and Freundlich models with maximum adsorption capacities of 97.47 and 99.70 mg/g respectively. Photocatalytic kinetic analysis confirmed that higher-temperature composites exhibited significantly greater rate constants, with Zn-Co-Oxide/CNH@800 recording the highest value of 0.01376 min^{-1}. The photocatalytic degradation efficiency was determined as Zn-Co-Oxide/CNH@900 (93%) > Zn-Co-Oxide/CNH@800 (92%) > Zn-Co-Oxide/CNH@700 (54%) > PAC@900 (33%) which indicated that the synergistic effect of metal incorporation and higher carbonization temperature was beneficial for photocatalytic efficiency. In summary, the results of this study show that the bimetallic MOF composites derived from Azolla have significant potential as materials for the removal of dyes and treatment of wastewater, which are sustainable and cost-efficient.

Limitations of the study

The present study was successful, but there are some limitations to be pointed out. The experiments were performed in controlled laboratory conditions with one single model dye, methylene blue, which is not as complex as real industrial waste water with mixtures of pollutants. Performance of the photocatalytic process under natural solar irradiation was not

tested and the intermediate degradation products produced during the photodegradation of methylene blue were not identified.

References

Ajmal, A., Majeed, I., Malik, R. N., Idriss, H., & Nadeem, M. A. (2014). Principles and mechanisms of photocatalytic dye degradation on TiO 2 based photocatalysts: a comparative overview. *Rsc Advances*, *4*(70), 37003-37026.

Alebachew Chekol, S., Nigussie, T. Z., & Fenta, B. A. (2024). Azolla as a beneficial macrophyte for livestock feed: a review. *Cogent Food & Agriculture*, *10*(1), 2367804.

Ali, H. (2010). Biodegradation of synthetic dyes—a review. *Water, Air, & Soil Pollution*, *213*(1), 251-273.

Ali, I. (2010). The quest for active carbon adsorbent substitutes: inexpensive adsorbents for toxic metal ions removal from wastewater. *Separation & Purification Reviews*, *39*(3-4), 95-171.

Ali, I. (2012). New generation adsorbents for water treatment. *Chemical reviews*, *112*(10), 5073-5091.

Alprol, A. E., Manaa, A., Basaham, A. S., Ghandour, I. M., El-Regal, M. A. A., & El-Metwally, M. E. (2025). Optimized removal of methylene blue from wastewater using an activated Carbon-Zinc Oxide-Ammonia composite. *Scientific Reports*, *15*(1), 38834.

Amalina, F., Abd Razak, A. S., Krishnan, S., Zularisam, A., & Nasrullah, M. (2022). Water hyacinth (Eichhornia crassipes) for organic contaminants removal in water–A review. *Journal of Hazardous Materials Advances*, *7*, 100092.

An, J., Nhung, N. T. H., Ding, Y., Chen, H., He, C., Wang, X., & Fujita, T. (2022). Chestnut shell-activated carbon mixed with pyrolytic snail shells for methylene blue adsorption. *Materials*, *15*(22), 8227.

Azizian, S., Eris, S., & Wilson, L. D. (2018). Re-evaluation of the century-old Langmuir isotherm for modeling adsorption phenomena in solution. *Chemical physics*, *513*, 99-104.

Beketov, M. A., Kefford, B. J., Schäfer, R. B., & Liess, M. (2013). Pesticides reduce regional biodiversity of stream invertebrates. *Proceedings of the National Academy of Sciences*, *110*(27), 11039-11043.

Berthomieu, C., & Hienerwadel, R. (2009). Fourier transform infrared (FTIR) spectroscopy. *Photosynthesis research*, *101*(2), 157-170.

Bethi, B., Sonawane, S. H., Bhanvase, B. A., & Gumfekar, S. P. (2016). Nanomaterials-based advanced oxidation processes for wastewater treatment: a review. *Chemical Engineering and Processing-Process Intensification*, *109*, 178-189.

Bhuvaneshwari, K., & Singh, P. K. (2015). Response of nitrogen-fixing water fern Azolla biofertilization to rice crop. *3 Biotech*, *5*(4), 523-529.

Bogyor, A., Csavdari, A. A., Lovász, T., & Bitay, E. (2025). A comparative kinetic and thermodynamic adsorption study of methylene blue and its analogue dye on filter paper. *International Journal of Molecular Sciences*, *26*(2), 516.

Boulkhessaim, S., Gacem, A., Khan, S. H., Amari, A., Yadav, V. K., Harharah, H. N., Elkhaleefa, A. M., Yadav, K. K., Rather, S.-u., Ahn, H.-J., & Jeon, B.-H. (2022). Emerging Trends in the Remediation of Persistent Organic Pollutants Using Nanomaterials and Related Processes: A Review. *Nanomaterials*, *12*(13), 2148. https://www.mdpi.com/2079-4991/12/13/2148

Burtch, N. C., Jasuja, H., & Walton, K. S. (2014). Water stability and adsorption in metal–organic frameworks. *Chemical reviews*, *114*(20), 10575-10612.

Chisanga, M., M'kandawire, E., Choongo, K., Kalunga, G., & Yabe, J. (2025). Assessment of total mercury (Hg) in soil, sediment, and tilapia fish (Oreochromis niloticus) and health risk assessment among residents of Kitwe mining area, Zambia. *Environmental Science and Pollution Research*, *32*(23), 13904-13917.

Chong, M. N., Jin, B., Chow, C. W., & Saint, C. (2010). Recent developments in photocatalytic water treatment technology: a review. *Water research*, *44*(10), 2997-3027.

Chung, K.-T. (2016). Azo dyes and human health: A review. *Journal of Environmental Science and Health, Part C*, *34*(4), 233-261.

Crini, G. (2006). Non-conventional low-cost adsorbents for dye removal: a review. *Bioresource technology*, *97*(9), 1061-1085.

Crini, G., & Badot, P.-M. (2008). Application of chitosan, a natural aminopolysaccharide, for dye removal from aqueous solutions by adsorption processes using batch studies: A review of recent literature. *Progress in polymer science*, *33*(4), 399-447.

Crini, G., & Lichtfouse, E. (2019). Advantages and disadvantages of techniques used for wastewater treatment. *Environmental chemistry letters*, *17*(1), 145-155.

Dagdag, O., Haldhar, R., Quadri, T. W., Daoudi, W., Berdimurodov, E., & Kim, H. (2024). Nanomaterials and Their Properties. In *Nano-Hybrid Smart Coatings: Advancements in Industrial Efficiency and Corrosion Resistance* (Vol. 1469, pp. 17-40). American Chemical Society. https://doi.org/doi:10.1021/bk-2024-1469.ch002

10.1021/bk-2024-1469.ch002

Das, M., Rahim, F. I., & Hossain, M. A. (2018). Evaluation of fresh Azolla pinnata as a low-cost supplemental feed for Thai Silver Barb Barbonymus gonionotus. *Fishes*, *3*(1), 15.

Devi, S., & Tyagi, S. (2022). Porous zinc-discs as nanocatalysts for methylene blue dye treatment in water: sensing, adsorption and photocatalytic degradation. *Rsc Advances*, *12*(54), 34951-34961.

El-Fattah, W. A., Guesmi, A., Hamadi, N. B., Alayyafi, A. A., & Shahat, A. (2024). Novel composite based on cellulose nanomaterial for detection and selective removal of cadmium (II) ions from wastewater. *Microchemical Journal*, *198*, 110175. https://doi.org/https://doi.org/10.1016/j.microc.2024.110175

Fang, Y., Zhou, S., Wang, Y., Yang, X., Ren, Y., Tang, K. H. D., & Li, R. (2025). Application of Biochar for the Removal of Dyes from Industrial Wastewater. *Biochar and the Circular Economy*, 156-167.

FAO. (2020). The State of Food and Agriculture 2020. Overcoming water challenges in agriculture. *Food and Agriculture Organization of the United Nations*.

Foo, K. Y., & Hameed, B. H. (2010). Insights into the modeling of adsorption isotherm systems. *Chemical engineering journal*, *156*(1), 2-10.

Forgacs, E., Cserháti, T., & Oros, G. (2004). Removal of synthetic dyes from wastewaters: a review. *Environment international*, *30*(7), 953-971.

Furukawa, H., Cordova, K. E., O'Keeffe, M., & Yaghi, O. M. (2013). The chemistry and applications of metal-organic frameworks. *Science*, *341*(6149), 1230444.

Ghamarpoor, R., Fallah, A., & Jamshidi, M. (2024). A Review of Synthesis Methods, Modifications, and Mechanisms of ZnO/TiO2-Based Photocatalysts for Photodegradation of Contaminants. *ACS Omega*, *9*(24), 25457-25492. https://doi.org/10.1021/acsomega.3c08717

Hamdan, H. Z., & Houri, A. F. (2022). CO2 sequestration by propagation of the fast-growing Azolla spp. *Environmental Science and Pollution Research*, *29*(12), 16912-16924.

Ho, Y.-S., & McKay, G. (1999). Pseudo-second order model for sorption processes. *Process biochemistry*, *34*(5), 451-465.

Hussein, E. B., & Rasheed, F. A. (2025). Sustainable removal of methylene blue from wastewater using silica sand coated with Al 2 O 3 nanoparticles: a comparative study of batch and fixed bed column reactors. *Rsc Advances*, *15*(59), 50829-50843.

Hussein, S. A., Taha, G. M., Adam, F., & Moghazy, M. A. (2025). Three different methods for ZnO-RGO nanocomposite synthesis and its adsorption capacity for methylene blue dye removal in a comparative study. *BMC chemistry*, *19*(1), 18.

Ibrahim, M. A., Salama, A., Zahran, F., Abdelfattah, M. S., Alsalme, A., Bechelany, M., & Barhoum, A. (2024). Fabrication of cellulose nanocrystals/carboxymethyl cellulose/zeolite membranes for methylene blue dye removal: Understanding factors, adsorption kinetics, and thermodynamic isotherms. *Frontiers in Chemistry*, *12*, 1330810.

Information, N. C. f. B. (2021). PubChem compound summary. In: National Center for Biotechnology Information Bethesda, MD, USA.

Iwuozor, K. O. (2019). Prospects and challenges of using coagulation-flocculation method in the treatment of effluents. *Advanced Journal of Chemistry-Section A*, *2*(2), 105-127.

Jack Clifton, I., & Leikin, J. B. (2003). Methylene blue. *American journal of therapeutics*, *10*(4), 289-291.

Jangid, P., & Prabhu Inbaraj, M. (2021). Applications of nanomaterials in wastewater treatment. *Materials Today: Proceedings*, *43*, 2877-2881. https://doi.org/https://doi.org/10.1016/j.matpr.2021.01.126

Järup, L. (2003). Hazards of heavy metal contamination. *British medical bulletin*, *68*(1), 167-182.

Jeffrey, K. B., Zheng, A. L. T., Hii, T. T., Seng, K. W. K., Chung, E. L. T., Lease, J., & Andou, Y. (2025). Sustainable dye wastewater treatment: Utilizing duckweed-derived adsorbents for efficient methylene blue removal. *Biomass Conversion and Biorefinery*, *15*(12), 19157-19173.

Jiang, X., Jia, Y., Ren, D., Zhang, N., Peng, T., & Huo, Z. (2023). Magnetic seeds promoted high-density sulfonic acid-based hydrochar derived from sugar-rich wastewater for

removal of methylene blue. *Environmental Science and Pollution Research*, *30*(13), 36872-36882.

Joseph, J., Radhakrishnan, R. C., Johnson, J. K., Joy, S. P., & Thomas, J. (2020). Ion-exchange mediated removal of cationic dye-stuffs from water using ammonium phosphomolybdate. *Materials Chemistry and Physics*, *242*, 122488.

Judd, S. J. (2017). Membrane technology costs and me. *Water research*, *122*, 1-9.

Kansara, N., Bhati, L., Narang, M., & Vaishnavi, R. (2016). Wastewater treatment by ion exchange method: a review of past and recent researches. *ESAIJ (Environmental Science, An Indian Journal)*, *12*(4), 143-150.

Kant, R. (2012). Textile dyeing industry an environmental hazard. *Natural science*, *4*(1), 22-26.

Kasperchik, V., Yaskevich, A., & Bil'Dyukevich, A. (2012). Wastewater treatment for removal of dyes by coagulation and membrane processes. *Petroleum Chemistry*, *52*(7), 545-556.

Kiani, D. (2023). X-ray diffraction (XRD). In *Springer Handbook of Advanced Catalyst Characterization* (pp. 519-539). Springer.

Konstantinou, I. K., & Albanis, T. A. (2004). TiO2-assisted photocatalytic degradation of azo dyes in aqueous solution: kinetic and mechanistic investigations: a review. *Applied Catalysis B: Environmental*, *49*(1), 1-14.

Korsa, G., Alemu, D., & Ayele, A. (2024). Azolla plant production and their potential applications. *International Journal of Agronomy*, *2024*(1), 1716440.

Kreno, L. E., Leong, K., Farha, O. K., Allendorf, M., Van Duyne, R. P., & Hupp, J. T. (2012). Metal–organic framework materials as chemical sensors. *Chemical reviews*, *112*(2), 1105-1125.

Kuppusamy, B., Mohamed Ismail, F. R., Balakrishnan, P., Kim, S.-C., Asrafali, S. P., & Periyasamy, T. (2026). From Biomass to Adsorbent: A Comprehensive Review on Bio-Derived Carbons for Dye Removal. *Polymers*, *18*(2), 180.

Kusumlata, Ambade, B., Kumar, A., & Gautam, S. (2024). Sustainable solutions: reviewing the future of textile dye contaminant removal with emerging biological treatments. *Limnological Review*, *24*(2), 126-149.

Landrigan, P. J., Fuller, R., Acosta, N. J., Adeyi, O., Arnold, R., Baldé, A. B., Bertollini, R., Bose-O'Reilly, S., Boufford, J. I., & Breysse, P. N. (2018). The Lancet Commission on pollution and health. *The lancet*, *391*(10119), 462-512.

Lanphear, B. P., Hornung, R., Khoury, J., Yolton, K., Baghurst, P., Bellinger, D. C., Canfield, R. L., Dietrich, K. N., Bornschein, R., & Greene, T. (2019). Erratum:"Low-level environmental lead exposure and children's intellectual function: an international pooled analysis". *Environmental health perspectives*, *127*(9), 099001.

Lei, Z., Sathish, C., Liu, Y., Karokoti, A., Wang, J., Qiao, L., Vinu, A., & Yi, J. (2022). Single metal atoms catalysts—Promising candidates for next generation energy storage and conversion devices. *EcoMat*, *4*(3), e12186.

Lellis, B., Fávaro-Polonio, C. Z., Pamphile, J. A., & Polonio, J. C. (2019). Effects of textile dyes on health and the environment and bioremediation potential of living organisms. *Biotechnology research and innovation*, *3*(2), 275-290.

Li, K., Zhang, X., Huang, X., Li, X., Chang, Q., Deng, S., & Zhu, G. (2024). MOF-on-MOF-derived FeZr bimetal oxides supported on hierarchically porous carbonized wood to promote photo-Fenton degradation of ciprofloxacin. *Journal of Water Process Engineering*, *63*, 105442.

Li, R., Wang, X., Lin, C., Zhang, X., & Yuan, Z. (2025). The synergistic effect of MOF and biomass achieving dual breakthroughs in material structure and performance. *Journal of Materials Chemistry A*, *13*(10), 6866-6894.

Lin, Z., Wang, R., Tan, S., Zhang, K., Yin, Q., Zhao, Z., & Gao, P. (2023). Nitrogen-doped hydrochar prepared by biomass and nitrogen-containing wastewater for dye adsorption: effect of nitrogen source in wastewater on the adsorption performance of hydrochar. *Journal of Environmental Management*, *334*, 117503.

Liu, H., Zhu, J., Li, Q., Li, L., Huang, Y., Wang, Y., Fan, G., & Zhang, L. (2023). Adsorption performance of methylene blue by KOH/FeCl3 modified biochar/alginate composite beads derived from agricultural waste. *Molecules*, *28*(6), 2507.

Liu, Q., Deng, W.-Y., Zhang, L.-Y., Liu, C.-X., Jie, W.-W., Su, R.-X., Zhou, B., Lu, L.-M., Liu, S.-W., & Huang, X.-G. (2023). Modified bamboo charcoal as a bifunctional material for methylene blue removal. *Materials*, *16*(4), 1528.

Lu, X.-M., Lu, P.-Z., & Yang, K. (2017). Restoration using Azolla imbricata increases nitrogen functional bacterial groups and genes in soil. *Applied microbiology and biotechnology*, *101*(9), 3849-3859.

Luo, L., Wu, X., Li, Z., Zhou, Y., Chen, T., Fan, M., & Zhao, W. (2019). Synthesis of activated carbon from biowaste of fir bark for methylene blue removal. *Royal Society open science*, *6*(9).

Ma, B., Zhu, J., Xu, Y., Zhang, L., Liu, D., Chen, C., & Sun, B. (2025). Photocatalytic degradation of methylene blue using ZnO modified with nano-biochar derived from bacterial cellulose. *Ceramics International*, *51*(11), 14948-14956.

Marsh, H., & Reinoso, F. R. (2006). *Activated carbon*. Elsevier.

Mcyotto, F., Wei, Q., Macharia, D. K., Huang, M., Shen, C., & Chow, C. W. (2021). Effect of dye structure on color removal efficiency by coagulation. *Chemical engineering journal*, *405*, 126674.

Meng, L., Shao, Z., Li, W., Wang, J., Hu, C., Yang, G., & Shi, Y. (2025). Study on the Mechanism and Modification of Carbon-Based Materials for Pollutant Treatment. *Materials*, *18*(23), 5345.

Mukhiya, T., Ojha, G. P., Dahal, B., Kim, T., Chhetri, K., Lee, M., Chae, S.-H., Muthurasu, A., Tiwari, A. P., & Kim, H. Y. (2020). Designed assembly of porous cobalt oxide/carbon nanotentacles on electrospun hollow carbon nanofibers network for supercapacitor. *ACS Applied Energy Materials*, *3*(4), 3435-3444.

Nandee, R., Chowdhury, M. A., Hossain, N., Rana, M. M., Mobarak, M. H., & Khandaker, M. R. (2024). Surface topography and surface morphology of graphene nanocomposite by FESEM, EDX and AFM analysis. *Nano-Structures & Nano-Objects*, *38*, 101170.

Nazri, M. K. H. M., & Sapawe, N. (2020). A short review on photocatalytic toward dye degradation. *Materials Today: Proceedings*, *31*, A42-A47.

Nosaka, Y., & Nosaka, A. Y. (2017). Generation and detection of reactive oxygen species in photocatalysis. *Chemical reviews*, *117*(17), 11302-11336.

Ogugbue, C. J., & Sawidis, T. (2011). Bioremediation and detoxification of synthetic wastewater containing triarylmethane dyes by Aeromonas hydrophila isolated from industrial effluent. *Biotechnology research international*, *2011*(1), 967925.

Organization, W. H. (2021). Progress on wastewater treatment: Global status and acceleration needs for SDG indicator 6.3. 1.

Paluch, D., Bazan-Wozniak, A., Nosal-Wiercińska, A., Cielecka-Piontek, J., & Pietrzak, R. (2024). Fennel seed biochar: A sustainable approach for methylene blue removal from aqueous solutions. *Materials*, *17*(17), 4350.

Pandey, K. (1999). A study of chemical structure of soft and hardwood and wood polymers by FTIR spectroscopy. *Journal of applied polymer science*, *71*(12), 1969-1975.

Patel, D., Tripathi, K. M., & Sonwani, R. K. (2024). Waste-Derived Carbon Nano-Onions for the Removal of Organic Dye from Wastewater and Phytotoxicity Studies. *ACS Omega*, *9*(28), 30834-30845. https://doi.org/10.1021/acsomega.4c03570

Pereira, A. L. (2017). The Unique Symbiotic System Between a Fern and a Cyanobacterium, Azolla-Anabaena azollae: Their potential as biofertilizer, feed, and remediation. *Symbiosis*, *60*(1), 1-10.

Periyasamy, A. P. (2024). Recent advances in the remediation of textile-dye-containing wastewater: prioritizing human health and sustainable wastewater treatment. *Sustainability*, *16*(2), 495.

Peters, G. A., & Mayne, B. C. (1974). The Azolla, Anabaena azollae relationship: I. Initial characterization of the association. *Plant Physiology*, *53*(6), 813-819.

Prüss-Ustün, A., Wolf, J., Bartram, J., Clasen, T., Cumming, O., Freeman, M. C., Gordon, B., Hunter, P. R., Medlicott, K., & Johnston, R. (2019). Burden of disease from inadequate water, sanitation and hygiene for selected adverse health outcomes: An updated analysis with a focus on low-and middle-income countries. *International journal of hygiene and environmental health*, *222*(5), 765-777.

Rakanović, M., Vukojević, A., Savanović, M. M., Armaković, S., Pelemiš, S., Živić, F., Sladojević, S., & Armaković, S. J. (2022). Zeolites as adsorbents and photocatalysts for removal of dyes from the aqueous environment. *Molecules*, *27*(19), 6582.

Ran, X., Wang, L., Xiao, B., Lei, L., Zhu, J., Liu, Z., Xi, X., Feng, G., Li, R., & Feng, J. (2022). Effective removal of methylene blue on EuVO4/g-C3N4 mesoporous nanosheets via coupling adsorption and photocatalysis. *International Journal of Molecular Sciences*, *23*(17), 10003.

Rashad, S. (2021). An overview on the aquatic fern Azolla spp. as a sustainable source of nutrients and bioactive compounds with resourceful applications. *Egyptian Journal of Aquatic Biology and Fisheries*, *25*(1), 775-782.

Saritha, V., Srinivas, N., & Srikanth Vuppala, N. (2017). Analysis and optimization of coagulation and flocculation process. *Applied Water Science*, *7*(1), 451-460.

Sevilla, M., & Fuertes, A. B. (2009). Chemical and structural properties of carbonaceous products obtained by hydrothermal carbonization of saccharides. *Chemistry–A European Journal*, *15*(16), 4195-4203.

Shabir, M., Yasin, M., Hussain, M., Shafiq, I., Akhter, P., Nizami, A.-S., Jeon, B.-H., & Park, Y.-K. (2022). A review on recent advances in the treatment of dye-polluted wastewater. *Journal of Industrial and Engineering Chemistry*, *112*, 1-19. https://doi.org/https://doi.org/10.1016/j.jiec.2022.05.013

Sharma, K., Rajan, S., & Nayak, S. K. (2024). Water pollution: Primary sources and associated human health hazards with special emphasis on rural areas. In *Water resources management for rural development* (pp. 3-14). Elsevier.

Sharma, S., & Kaur, A. (2018). Various methods for removal of dyes from industrial effluents-a review. *Indian J. Sci. Technol*, *11*(12), 1-21.

Singh, D., & Fulekar, M. (2010). Benzene bioremediation using cow dung microflora in two phase partitioning bioreactor. *Journal of Hazardous Materials*, *175*(1-3), 336-343.

Sundararaman, S., Senthil Kumar, P., Deivasigamani, P., Jagadeesan, A. K., Devaerakkam, M., Al-Hashimi, A., & Choi, D. (2021). Assessing the plant phytoremediation efficacy for Azolla filiculoides in the treatment of textile effluent and redemption of Congo red dye onto Azolla biomass. *Sustainability*, *13*(17), 9588.

Sutton, M. A., Oenema, O., Erisman, J. W., Leip, A., Van Grinsven, H., & Winiwarter, W. (2011). Too much of a good thing. *Nature*, *472*(7342), 159-161.

Tan, X., Liu, Y., Zeng, G., Wang, X., Hu, X., Gu, Y., & Yang, Z. (2015). Application of biochar for the removal of pollutants from aqueous solutions. *Chemosphere*, *125*, 70-85.

Torres, E. (2020). Biosorption: A review of the latest advances. *Processes*, *8*(12), 1584.

Türgay, O., Ersöz, G., Atalay, S., Forss, J., & Welander, U. (2011). The treatment of azo dyes found in textile industry wastewater by anaerobic biological method and chemical oxidation. *Separation and Purification Technology*, *79*(1), 26-33.

Turner, S. W. D., Rice, J. S., Nelson, K. D., Vernon, C. R., McManamay, R., Dickson, K., & Marston, L. (2021). Comparison of potential drinking water source contamination across one hundred U.S. cities. *Nature Communications*, *12*(1), 7254. https://doi.org/10.1038/s41467-021-27509-9

Vigdorowitsch, M., Pchelintsev, A., Tsygankova, L., & Tanygina, E. (2021). Freundlich isotherm: An adsorption model complete framework. *Applied sciences*, *11*(17), 8078.

Vijayan, K., Deepthi, K., & Reshma, C. (2024). Exploring the multifaceted benefits of Azolla: A comprehensive review of an aquatic fern's biological and practical contributions. *International Journal of Ecology and Environmental Sciences*, *50*(5), 661-672.

Wang, J., Tan, Y., Yang, H., Zhan, L., Sun, G., & Luo, L. (2023). On the adsorption characteristics and mechanism of methylene blue by ball mill modified biochar. *Scientific Reports*, *13*(1), 21174.

Ward, M. H., Jones, R. R., Brender, J. D., De Kok, T. M., Weyer, P. J., Nolan, B. T., Villanueva, C. M., & Van Breda, S. G. (2018). Drinking water nitrate and human health: an updated review. *International journal of environmental research and public health*, *15*(7), 1557.

Water, U. (2020). Water and climate change. *The United Nations World Water Development Report*.

Wei, Y., Fu, Z., Meng, Y., Li, C., Yin, F., Wang, X., Zhang, C., Guo, L., & Sun, S. (2024). Photocatalytic degradation of methylene blue over MIL-100 (Fe)/GO composites: a performance and kinetic study. *International Journal of Coal Science & Technology*, *11*(1), 42.

WHO. (2019). Drinking Water: Key Facts. In: World Health Organization Geneva.

Yagub, M. T., Sen, T. K., Afroze, S., & Ang, H. M. (2014). Dye and its removal from aqueous solution by adsorption: a review. *Advances in colloid and interface science*, *209*, 172-184.

Yahya, M. A., Al-Qodah, Z., & Ngah, C. Z. (2015). Agricultural bio-waste materials as potential sustainable precursors used for activated carbon production: A review. *Renewable and sustainable energy reviews*, *46*, 218-235.

Yunusa, U., Usman, B., & Ibrahim, M. B. (2021). Cationic dyes removal from wastewater by adsorptive method: A systematic in-depth review. *Algerian Journal of Chemical Engineering*, *1*(2), 6-40.

Yusuf, M. (2019). Synthetic dyes: a threat to the environment and water ecosystem. *Textiles and clothing*, 11-26.

Zhang, F., Liu, Y., Lei, J., Wang, S., Ji, X., Liu, H., & Yang, Q. (2019). Metal–organic-framework-derived carbon nanostructures for site-specific dual-modality photothermal/photodynamic thrombus therapy. *Advanced science*, *6*(17), 1901378.

Zhang, M., Xiao, C., Zhang, C., Qi, J., Wang, C., Sun, X., Wang, L., Xu, Q., & Li, J. (2020). Large-scale synthesis of biomass@ MOF-derived porous carbon/cobalt nanofiber for environmental remediation by advanced oxidation processes. *ACS ES&T Engineering*, *1*(2), 249-260.

Zhang, P., Shen, Z., Jia, L., & Qiu, J. (2026). Biomass-Derived Carbon for Boosting Photocatalysis. *Small*, *22*(8), e12210.

Zou, H., Wang, F., Zeng, Z., Zhu, J., Zha, L., Huang, D., Li, J., & Wang, R. (2025). Next-generation water-saving strategies for greenhouses using a nexus approach with modern technologies. *Nature Communications*, *16*(1), 2091. https://doi.org/10.1038/s41467-025-57388-3

Appendix

Appendix I Herbarium of plant and its identification

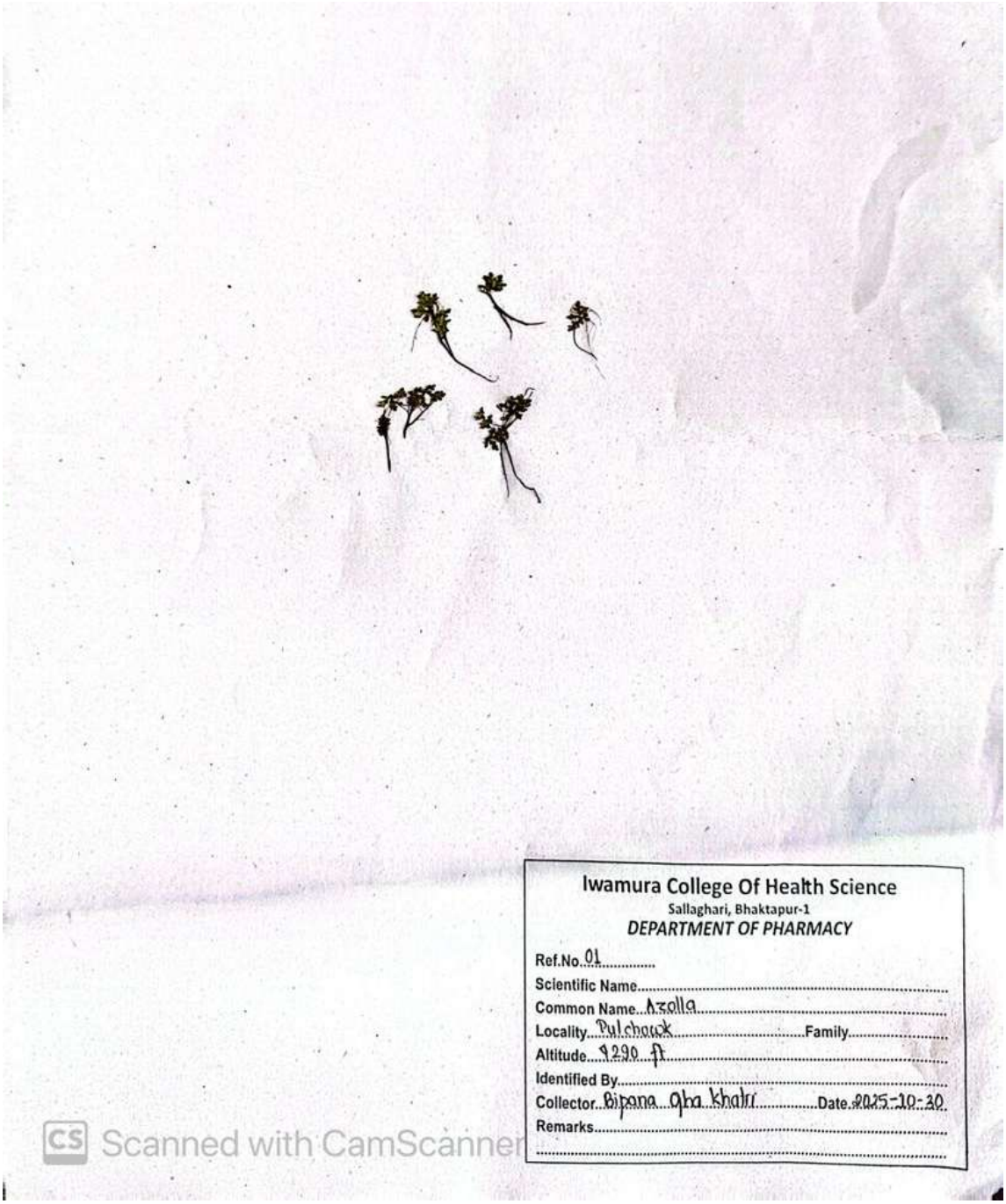

प्राविधिक विशेषज्ञको प्रतिवेदन

१. नमूना परिक्षण गर्न पठाउने व्यक्ति/निकायः- श्री बिपना ओझा खत्री, पुल्चोक क्याम्पस, पुल्चोक, ललितपुर।

२. प्राप्त नमूनाको विवरणः- वनस्पतिका नमूनाहरु थान -४

३. यस कार्यालयमा प्राप्त मितिः- २०८२/०८/१७

४. परिक्षणका आधारहरुः- (क) हर्बेरियममा भएको नमूनाहरु संगको तुलनात्मक अध्ययन ।
(ख) सन्दर्भ सामग्रीहरुको अध्ययन ।

५. पहिचान प्रतिवेदनः- प्राप्त नमूनाको Morphological अध्ययन र यस राष्ट्रिय हर्बेरियम तथा वनस्पति प्रयोगशालाको हर्बेरियममा राखिएका नमूनाहरु संगको तुलनात्मक अध्ययन गर्दा उक्त नमूना निम्नानुसार भएको पहिचान हुन गएको।

S. No	Scientific Name	Family	Remarks
1	*Chromolaena odorata* (L.) R.M.King & H.Rob	Asteraceae	
2	*Lantana camara* L.	Verbenaceae	
3	*Azolla pinnata* R.Br.	Salviniaceae	
4	*Jacaranda mimosifolia* D.Don	Bignoniaceae	

६. परिक्षण गर्ने अधिकारीः-

२०८२/८/१७

सजिता ढकाल
अनुसन्धान अधिकृत
(२२५७०४)

Appendix II Paper presentation of the work at IOE graduation conference

971

IOE Graduate Conference

Certificate of Participation

This certificate is awarded to

Bipana Ojha Khatri

in recognition of an invaluable contribution to
the academic discourse and research dessimination
at the 18th IOE Graduate Conference held from May 7 to 9, 2026
organized by Pulchowk Campus, Lalitpur, Nepal
through the Paper Presentation entitled

"Azolla-based Zinc-Cobalt Integrated Carbon for Methylene Blue Degradation."

Prof. Sangeeta Singh
Conference Convener

Prof. Sanjay Uprety
Campus Chief, Pulchowk Campus

Prof. Sushil Bahadur Bajracharya
Dean, Institute of Engineering

Appendix III Poster presentation at Third International Conference on Heritage, Innovation and Transformation

Certificate of Presentation

This is to certify that

BIPANA OJHA KHATRI

Department of Applied Sciences and Chemical Engineering, Pulchowk Campus, Tribhuvan University

for presenting poster on

Bimetallic MOF-Derived Carbon from Azolla Biomass for Photocatalytic Dye Degradation

at

Third International Conference on
Heritage, Innovation and Transformation

17-19 February 2026 at Far Western University, Mahendranagar, Kanchanpur, Nepal

Organized by

Far Western University, Nepal

Co-organized by

Nepal Materials Science Society, Nepal

Hon'ble Nazir Miya	Prof. Hem Raj Pant, PhD	Prof. Binod Lekhak, PhD	Prof. Kishan Datta Bhatta, PhD
Governor	Vice Chancellor	Registrar	Conference Convener
Sudurpaschim Province	Far Western University	Far Western University	Far Western University

Appendix IV Photographs taken during presentation